Rotational bands in ^{133}Nd

D. Bazzacco, F. Brandolini, G. Falconi, S. Lunardi, N. H. Medina,* P. Pavan, and C. Rossi Alvarez

Dipartimento di Fisica dell' Universitá and INFN, Sezione di Padova, Padova, Italy

G. de Angelis, D. De Acuna, M. De Poli, D. R. Napoli, and J. Rico

INFN, Laboratori Nazionali di Legnaro, Legnaro, Italy

D. Bucurescu, M. Ionescu-Bujor, and C. A. Ur

National Institute of Physics and Nuclear Engineering, Bucharest, Romania

The high-spin structure of the nucleus ^{133}Nd has been studied with the GASP array using the ^{104}Pd(^{32}S,$2pn$) and ^{105}Pd(^{32}S,$2p2n$) reactions. The observed levels have been organized into nine rotational bands including the well-known highly deformed band which has been linked to the states at normal deformation. The bands, which have been classified as being built on different Nilsson orbitals, are discussed in the framework of the interacting boson fermion, particle-plus-triaxial rotor, and cranked shell models. [S0556-2813(98)05110-3]

PACS number(s): 21.10.Re, 21.60.−n, 23.20.Lv, 27.60.+j

I. INTRODUCTION

After the first superdeformed (SD) band identification in ^{132}Ce [1], many other bands characterized by narrow (≈ 70 keV) and fairly regular energy spacings have been discovered in the nuclei of the mass $A=130$ region [2,3]. Such bands arise from a second minimum in the potential energy surface, corresponding to prolate shapes with $\beta_2 = 0.35–0.40$, whereas the first minimum has a deformation $\beta_2 = 0.20–0.25$ [4]. They are also often called highly deformed (HD) bands (as we will do in the present paper) in order to emphasize their smaller deformation with respect to the SD bands in the $A=80$, 150, 190 regions ($\beta_2 \approx 0.5–0.6$).

The study of HD band properties in the mass $A=130$ region has attracted much interest, and by now a lot of data is available on such bands in the whole region. In many cases, the discovery of the HD bands in a particular nucleus has preceded a detailed spectroscopy study of the same nucleus at normal deformation. This was the case of ^{133}Nd where, beside the HD band, which has been the object of many studies [2,5–8], only few γ rays assigned to the decay of levels with spins and parities given just on the basis of systematics were known [9]. The complicated decay out of the HD bands, together with the poor knowledge of the level scheme at low energy, was the main reason which prevented for a long time the identification of the decay out of the HD bands toward normally deformed (ND) states in the mass $A=130$ region.

The ^{133}Nd nucleus was the one with the largest reported population of a HD band in the $A=130$ region [2] and we therefore chose it as the best candidate for the search of a clear connection between HD and ND states. Experiments have been carried out at the GASP array, with the goal to establish a level scheme as complete as possible for ^{133}Nd at normal deformation and to find the transitions linking the

HD band to the rest of the level scheme. Indeed, such linking transitions have been found allowing the spin-parity assignments for the HD band. The results on the decay out have been already published in form of letters [10,11].

Several rotational bands, at lower deformation, have been found in ^{133}Nd during the course of this study. They could be followed up to relatively high spins and excitation energies. Preliminary reports on some of these structures have been given already in Refs. [10,11]. In this paper, a full account of the experimental results on rotational bands in the ^{133}Nd nucleus will be presented.

The HD band has been interpreted through the occupation by the 73rd neutron of the [660]1/2 Nilsson orbital (arising from the $\nu i_{13/2}$ spherical j shell) which is strongly downsloping and approaches the Fermi surface at high deformation ($\beta_2 = 0.35$). In a first approach, also the other rotational bands can be classified, according to the Nilsson scheme, as being built on the various orbitals available to the odd neutron at normal deformation. This description, based on axially symmetric rotor, can be anyway too simple and may not be able to reproduce all the properties of the bands. It is known in fact that ^{133}Nd belongs to a region of transitional nuclei in which the γ degree of freedom plays an important role. About 20 years ago the triaxial-core model of Meyer-ter-Vehn [12] has been applied to describe the low-lying negative-parity bands built on the $h_{11/2}$ neutron orbital known in several odd-mass Ba [13,14], Ce [15], and Nd [9,12] nuclei with mass number $A \approx 130$ and a significant departure from axial symmetry has been established. These nuclei are characterized by softness with respect to the γ deformation and therefore shape polarization could occur due to the particles occupying different orbitals. Recently, it has been shown that the γ-soft nuclei of the $A=130$ region can be satisfactorily described by assuming a rigid triaxial core characterized by an average γ value [16]. A detailed analysis of the observed properties of the low-lying bands in the odd-mass neutron-deficient Xe, Ba [17,18], and Ce [19] nuclei have been performed within the particle-plus-triaxial rotor model (PTRM) of Ref. [20] and large triaxial deformations with γ in the range $15°–30°$ have been established for

*Permanent address: Departamento de Fisica Nuclear, University of Sao Paulo, Sao Paulo, Brazil.

the negative-parity structures and, in some cases, also for the positive-parity structures.

An alternative to the particle-triaxial rotor model description is offered by the interacting boson fermion model (IBFM) [21]. This model was recently applied in the $A \approx 130$ mass region to the neutron-deficient isotopes of Xe [22], Ba [23], and Ce [24]. It is of interest to compare the description provided for the low-lying structures of ^{133}Nd by these two different approaches, and for this purpose calculations were performed using both the interacting boson fermion and particle-plus-triaxial-rotor models. As concern the high-spin states, the discussion is based on the the cranked shell model (CSM), following a procedure similar to that recently applied to the ^{129}Ba isotone [25].

II. MEASUREMENTS AND RESULTS

Two independent experiments have been performed in order to study rotational bands in ^{133}Nd. In the first one, a 155 MeV ^{32}S beam was bombarding a thin ^{105}Pd target consisting of two self-supporting foils for a total thickness of 1 mg/cm^2 (from here on "thin target experiment"). In the second one, the reaction ^{104}Pd+^{32}S at 135 MeV has been used and the target consisted of 1.1 mg/cm^2 of ^{104}Pd evaporated on a 15 mg/cm^2 gold foil (thick target experiment). A different reaction has been chosen in the second experiment instead of the ^{32}S+^{105}Pd one because exploratory runs have shown that the channel of interest, namely ^{133}Nd, was populated in a cleaner way. The beam was provided by the Tandem XTU accelerator of Legnaro and γ rays have been detected using the GASP array which in its standard configuration consists of 40 high efficiency Compton suppressed germanium detectors and of a bismuth germanate (BGO) inner ball acting as multiplicity filter and total-energy spectrometer. In the thin target experiment the number of installed Ge detectors was 31, while in the thick target one it was 38. In this second case also two planar germanium detectors were used for the detection of low-energy γ rays. Events were collected when at least three suppressed Ge detectors and three detectors of the inner ball fired in coincidence. With such conditions the event rate was ranging from 5 to 7 kHz by keeping a singles rate in the germanium detectors of 8–10 kHz. The beam current was 4 and 10 pnA in the thick and thin target experiments, respectively. After unfolding the stored events, 2×10^9 and 1.2×10^9 triples coincidences data were available for the off-line analysis in the thin and thick target experiments, respectively.

Energy calibrations of the spectra and gain matching between the different Ge detectors have been performed using standard γ-ray sources as well as known γ-ray transitions of the nuclei populated in the reactions. The data have been sorted into fully symmetrized matrices and cubes with proper conditions on the fold and on the sum energy of the BGO ball. In order to enhance the different band structures seen in ^{133}Nd, we made use of the triples data by constructing γ-γ matrices in coincidence with the strongest transitions in each observed rotational band. Examples of doubly gated spectra showing various rotational sequences in ^{133}Nd are given in Figs. 1 and 2 for the thick target and thin target experiments, respectively. As it is evident from Fig. 1 the thick target data, which have been essential in constructing the low spin part

of the level scheme, limit the observation of high-spin states up to spin$\approx$20. The thin target data on the other side have allowed us to extend the observation of levels in ^{133}Nd up to spin $89/2^+$, which is the highest in the HD band.

The spins and parities of the levels have been deduced from the analysis of the directional correlation ratios from oriented states (DCO) [26] for the ^{133}Nd transitions. A DCO γ-γ matrix has been created sorting on one axis the detectors lying at 90° with respect to the beam direction and on the other those at 34° and 146°. In the GASP geometry, if one sets a gate on a stretched quadrupole transition, the theoretical DCO ratios $I_{90°}(\gamma)/I_{34°}(\gamma)$ are $\approx$1 for stretched quadrupole transitions and $\approx$0.5 for pure dipole ones. If, on the contrary, gates are set on a pure dipole transition, the expected DCO ratios for quadrupole and dipole transitions are 2 and 1, respectively. Obviously, if the transition of interest is of mixed dipole/quadrupole character, different values are obtained depending on the sign and value of the mixing ratio δ [26].

The energies and relative intensities of the γ transitions belonging to ^{133}Nd, together with the DCO ratios and the spin-parity assignments are reported in Table I. The relative intensities of the low-lying transitions were determined from the total projection of the thick target experiment and normalized to the 162.9 keV $11/2^- \rightarrow 9/2^-$ transition. For the transitions lying at higher excitation energy, the relative intensities are extracted from gated spectra. For weak or contaminated transitions and some of those linking different bands it has not been possible to deduce the intensity values. In Table I, for the sake of clarity, the γ-ray transitions are arranged according to their placement in the level scheme of Fig. 3 and/or their character (in-band transitions, transitions connecting different bands).

III. THE LEVEL SCHEME OF ^{133}Nd

The level scheme of the ^{133}Nd nucleus deduced from the present study is shown in Figs. 3(a) and 3(b). It is organized into nine different structures labeled from 1 to 9. Negative-parity bands are presented in Fig. 3(a), whereas the positive parity bands are displayed in Fig. 3(b). The HD band (band 5) is shown in both figures together with its decay out to both negative- and positive-parity states.

The transitions have been placed in the level scheme on the basis of coincidence relationships and relative intensities. Spin assignments are based on DCO analysis and on decay patterns. The parity of the levels has been established assuming that, when gating on a $\Delta I = 2$ stretched quadrupole transition, the strong transitions with DCO ratios $\approx$1 have $E2$ character and the transitions with DCO ratios definitely different from 1 and 0.5 are of mixed multipolarity ($M1 + E2$ character).

Apart from the HD band, only a strongly populated band, that from systematics was assigned to have negative parity and be based on a $9/2^-$ state [9], was known in ^{133}Nd before our study began. In our thick target experiment we could observe that this band is built on an isomeric state which decays with $T_{1/2} = 301 \pm 18$ ns through a 176 keV transition (see Fig. 4). An analogous isomer is known in the ^{131}Ce isotone where the $9/2^-$ state (on which a similar negative-parity band is built) has a half-life of 80 ns and decays
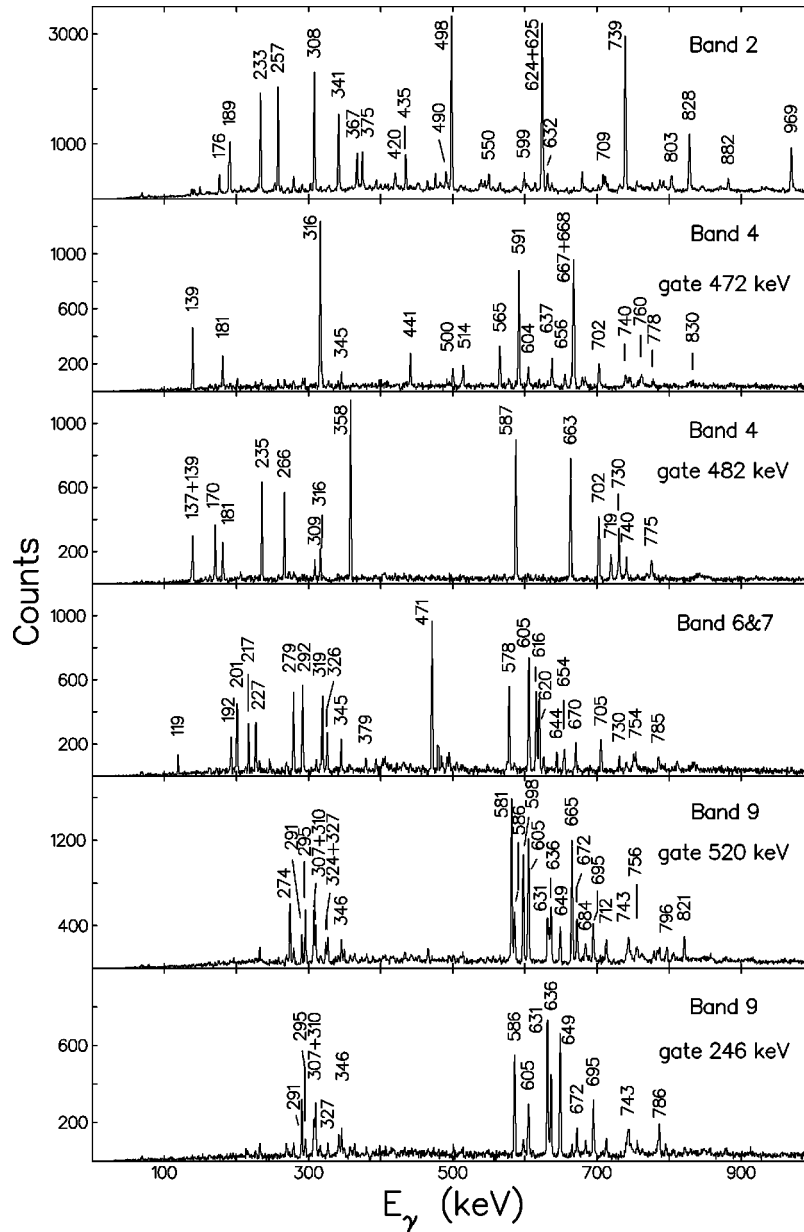
FIG. 1. Doubly gated coincidence spectra, from the thick target experiment, showing the low energy part of some rotational bands in ^{133}Nd. They were obtained by summing the spectra resulting from various combinations of twofold gates on clean transitions belonging to each band. When a gate is indicated, that transition's energy is always entering in the double-gate condition.

through a 162 keV transition to the $7/2^+$ ground state [27]. In this way we have assumed a $7/2^+$ ground state also in ^{133}Nd.

Of great help in confirming the low-energy part of the level scheme has been the recent, parallel β-decay study of ^{133}Pm [28] performed at Georgia Institute of Technology. In this study a spin-parity $7/2^+$ is assigned to the ^{133}Nd ground state and furthermore a new β^+ decaying state with spin $1/2^+$ was identified at 128 keV. We had in fact the puzzling situation that the two signature partners of band 6, the one getting the higher feeding from the decay of the HD band, were terminating, at low spin, 128 and 173 keV above the ground state, respectively. And in fact, the β^+ study shows also a 45 keV transition (not seen in our experiment) connecting a $3/2^+$ state at 173 keV to the $1/2^+$ β^+ decaying state. The electron conversion data [28] together with our DCO ratios allow for an unambiguous spin-parity assign-

ment for all the relevant low-spin states (up to $E_x \approx 500$ keV) of ^{133}Nd. In the low-spin part of the band 4 three levels ($3/2^-$, $5/2^-$, and $7/2^-$) are in common with the β-decay work. In our experiment we have found a weak 137 keV transition deexciting the $5/2^-$ level. Although the DCO ratio for this transition could not be determined we interpret the new level as the missing $1/2^-$ member of the band, expected near the $3/2^-$ state and in fact lying only 33 keV above. This ($1/2^-$) level decays through a 259 keV transition to the $1/2^+$ β-decaying isomer.

Beside the $T_{1/2} = 301$ ns isomeric state at 176 keV, also the $3/2^-$ state at 353.6 keV exhibits a half-life in the ns range. It has been measured in [28] as $T_{1/2} = 46$ ns. Because of the presence of the isomer the intensity of the 181 keV transition, derived from coincidence data, results much lower than the intensity of the transitions populating the isomer
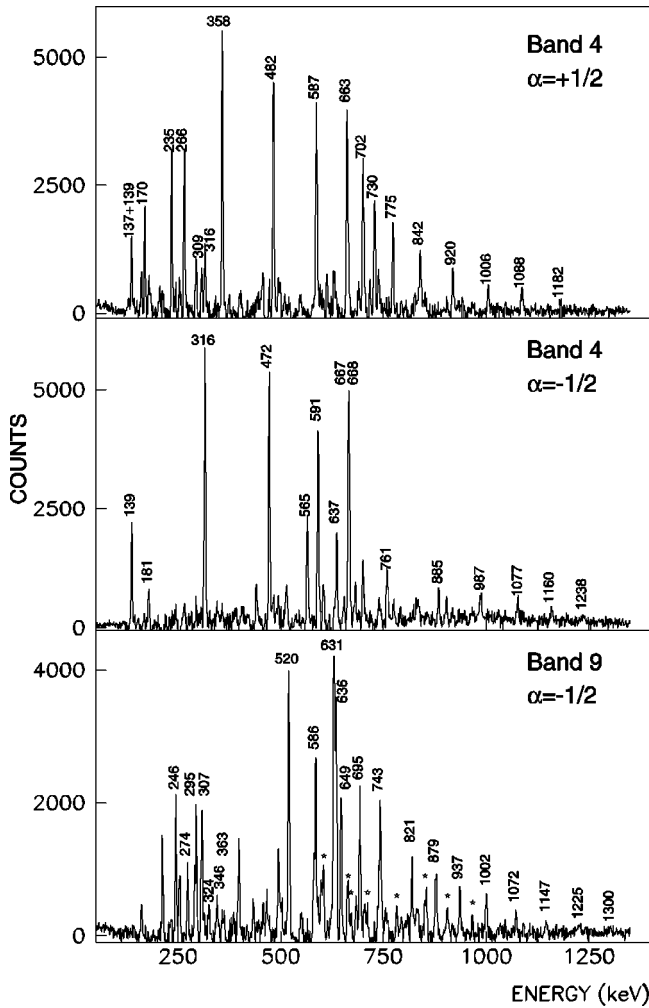
FIG. 2. Doubly gated coincidence spectra, from the thin target experiment, showing the extension to high energy of some of the bands of ¹³³Nd. They were obtained by summing the spectra resulting from various combinations of twofold gates on clean transitions belonging to each band. The stars in the lowest spectrum indicate the $E2$ transitions from the $\alpha = +1/2$ member of band 9, seen through the $\Delta I = 1$ transitions which connect the two signature partners of band 9.

(see Table I). Time spectra obtained by gating on the 181 keV transition indicate clearly the presence of this isomer with a half-life consistent with the value given in [28].

For the states above 500 keV, which are members of regular rotational bands, spins and parities are straightforward from DCO ratios. They are in fact ≈1 for all in-band $E2$ transitions and ≈0.5 for the $M1$ transitions connecting signature partners bands (see Table I). Exceptions to this rule are the 225, 334, 397, and 422 $\Delta I = 1$ transitions of the band 6 and the 170, 266, and 309 $\Delta I = 1$ transitions of the band 4 which all have large DCO ratios explained by a mixed $E2/M1$ character with rather large δ values (0.3–0.4).

Spin, parity, and absolute excitation energy of the HD band levels could be determined in this work through the identification of 10 transitions linking the HD band to normally deformed states of both positive and negative parity. They are listed in Table I together with their intensities and DCO ratios which result in unambiguous spin-parity assignment for the HD band levels. The mechanism of the decay

out of the HD band has been already discussed in detail in Refs. [10,11].

From the γ-ray intensities reported in Table I we have revaluated the relative intensity of the HD band with respect to the total population of the ¹³³Nd nucleus, which results now to be ≈6.5%. This value is comparable with those of similar bands in odd-even nuclei of the mass $A = 130$ region and much lower than the ≈20% value earlier reported [2], derived when the knowledge of the ¹³³Nd level scheme was much poorer.

IV. DISCUSSION

The low-spin states of ¹³³Nd populated in the β decay of ¹³³Pr have been recently discussed [28] in the framework of the particle-plus-triaxial rotor model. The calculations were performed by using, for the deformed mean field, a Woods-Saxon potential with a quadrupole deformation parameter $\beta_2 = 0.256$ under the assumption of axial symmetry ($\gamma = 0°$) and a good qualitative description of the experimental low-energy spectrum was obtained. The experimental band-heads could be readily identified with the calculated ones, characterized by the Nilsson labels which are dominant in their wave function (see Fig. 8 of Ref. [28]). The same labels are reported in our Figs. 3(a) and 3(b), which characterize now regular rotational bands built on specific Nilsson orbitals. Only at high spins, a new (with respect to the β-decay study) regular rotational band appears which is interpreted as being built on the $[660]1/2 \, \nu i_{13/2}$ intruder orbital. Some discrepancies between the experimental features (relative position of the bandheads, signature splitting of some low-lying states) and the calculated ones have been already noticed in [28] indicating that an improvement of the mean-field description is necessary and/or that the observed structures could have triaxial shapes. Before going into a detailed discussion of the properties of the various bands in the frame of the IBFM, PTRM, and CSM, we would like to point out the similarity of the level structure of the odd-N nucleus ¹³³Nd ($N = 73$) with the corresponding odd-Z nuclei with $Z = 73$. In fact, very similar band structures have been seen in ¹⁷¹,¹⁷³Ta based on the $[402]5/2^+$, $[404]7/2^+$, $[411]1/2^+$, $[514]9/2^-$, $[541]1/2^-$ and $[660]1/2^+$ Nilsson orbitals [29,30].

A. IBFM description of the low-lying states

As already mentioned in the Introduction, the interacting boson fermion model was recently applied to the neutron deficient isotopes of Xe [22], Ba [23], and Ce [24]. A reasonable description of the low-lying states of both parities in these nuclei has been achieved within the model by coupling a neutron which can occupy essentially the ''valence'' orbitals $1g_{7/2}$, $2d_{5/2}$, $3s_{1/2}$, $2d_{3/2}$, and $1h_{11/2}$, to the states of the even-even core described by the interacting boson model. In describing the isotonic Ba and Ce nuclei, it was found that the same set of model parameters could be used [24]. It was therefore interesting to see to which extent the same parameters are able to predict the properties of Nd isotopes. With this purpose, we have performed an IBFM-1 calculation for the positive parity states in ¹³³Nd in which we have adopted an approach similar to that for its isotones ¹²⁹Ba and ¹³¹Ce [23,24].

TABLE I. Energies, relative intensities, and DCO ratios of γ-ray transitions assigned to ^{133}Nd from the reactions used in this experiment. The intensities are normalized to that of the 162.9 keV transition (assumed to be 1000). Errors in the γ-ray energies are below 0.2 keV for strong transitions, and up to 1 keV for the weakest transitions on top of the bands. The DCO ratios are obtained by gating on stretched $\Delta I = 2$ transitions, unless otherwise stated.

E_γ (keV)	E_i (keV)	I_i	I_f	Intensity	R_{DCO}
Band 1					
$\alpha = +1/2$					
370.9	3401.9	$29/2^-$	$25/2^-$		
598.6	4000.7	$33/2^-$	$29/2^-$	110(10)	
786.9	4787.5	$37/2^-$	$33/2^-$	50(5)	
934.3	5722	$41/2^-$	$37/2^-$	25(5)	
1022.9	6745	$45/2^-$	$41/2^-$	25(5)	
$\alpha = -1/2$					
490.2	3659.3	$31/2^-$	$27/2^-$	90(10)	1.1(2)
708.5	4367.7	$35/2^-$	$31/2^-$	70(5)	0.8(2)
871.1	5238.6	$39/2^-$	$35/2^-$	70(5)	1.4(4)
$\Delta I = 1$ *transitions*					
137.6	3168.9	$27/2^-$	$25/2^-$	28(5)	
233.0	3401.9	$29/2^-$	$27/2^-$	340(10)[a]	0.56(6)
257.4	3659.3	$31/2^-$	$29/2^-$	240(10)	0.53(6)
341.4	4000.7	$33/2^-$	$31/2^-$	230(10)	0.42(6)
367.0	4367.7	$35/2^-$	$33/2^-$	145(10)	0.40(6)
419.8	4787.5	$37/2^-$	$35/2^-$	70(5)	
451.1	5238.6	$39/2^-$	$37/2^-$	60(5)	
482.9	5722	$41/2^-$	$39/2^-$	40(5)	
Other transitions related to band 1					
302.6	4406.1			30(5)	
588.1	3401.9	$29/2^-$	$25/2^-$	170(5)	
701.6	4103.5		$29/2^-$	30(5)	
Band 2					
$\alpha = +1/2$					
470.5	647.0	$13/2^-$	$9/2^-$	145(8)	1.5(2)
625.0	1272.0	$17/2^-$	$13/2^-$	190(10)	
738.9	2010.9	$21/2^-$	$17/2^-$	150(10)	1.2(1)
802.8	2813.7	$25/2^-$	$21/2^-$	104(5)	1.0(2)
754.9	3568.6	$29/2^-$	$25/2^-$	55(5)	0.9(9)
$\alpha = -1/2$					
498.3	837.5	$15/2^-$	$11/2^-$	650(25)	1.2(1)
623.5	1461.0	$19/2^-$	$15/2^-$	685(25)	0.98(3)
738.9	2199.9	$23/2^-$	$19/2^-$	665(23)	1.1(1)
827.8	3027.7	$27/2^-$	$23/2^-$	310(12)	0.95(6)
881.9	3909.6	$31/2^-$	$27/2^-$	70(5)	0.8(2)
776.0	4685.6	$35/2^-$	$31/2^-$	30(5)	0.8(2)
805.7	4715.3		$31/2^-$	15(5)	
$\Delta I = 1$ *transitions*					
162.9	339.2	$11/2^-$	$9/2^-$	1000	0.44(3)
307.8	647.0	$13/2^-$	$11/2^-$	350(15)	0.41(3)
190.6	837.5	$15/2^-$	$13/2^-$	190(7)	0.48(2)
434.5	1272.0	$17/2^-$	$15/2^-$	115(6)	0.27(6)
188.9	1461.0	$19/2^-$	$17/2^-$	40(3)	
550.0	2010.9	$21/2^-$	$19/2^-$	60(4)	0.33(6)
189.0	2199.9	$23/2^-$	$21/2^-$	20(5)	
614.0	2813.7	$25/2^-$	$23/2^-$	50(4)	
214.0	3027.7	$27/2^-$	$25/2^-$	20(5)	
541.1	3568.6	$29/2^-$	$27/2^-$	15(3)	
Band 3					
539	1186	$15/2^-$	$13/2^-$	80(10)	0.2(1)
630	1816	$19/2^-$	$15/2^-$	80(10)	2.3(9)[b]
712	2528.0	$23/2^-$	$19/2^-$	80(10)	0.96(5)

TABLE I. (*Continued*).

E_γ (keV)	E_i (keV)	I_i	I_f	Intensity	R_{DCO}
Band 4					
$\alpha = -1/2$					
138.9	492.6	$7/2^-$	$3/2^-$	75(5)	1.50(15)
316.0	808.6	$11/2^-$	$7/2^-$	225(15)	0.88(2)
472.4	1281.0	$15/2^-$	$11/2^{-1}$	225(15)	1.05(3)
591.4	1872.4	$19/2^-$	$15/2^-$	215(15)	0.96(3)
666.8	2539.2	$23/2^-$	$19/2^-$	185(15)	0.94(3)
668.2	3207.4	$27/2^-$	$23/2^-$	185(15)	
565.0	3772.4	$31/2^-$	$27/2^-$	155(10)	1.1(1)
637.3	4409.7	$35/2^-$	$31/2^-$	115(10)	0.8(3)
760.5	5170	$39/2^-$	$35/2^-$	51(5)	1.1(3)
884.6	6055	$43/2^-$	$39/2^-$	27(3)	1.0(3)
987.0	7042	$47/2^-$	$43/2^-$	25(3)	
1076.9	8119	$51/2^-$	$47/2^-$	18(9)	
1159.6	9278	$55/2^-$	$51/2^-$	10(5)	
1238.0	10516	$59/2^-$	$55/2^-$	10(5)	
Other transitions related to band 4 ($\alpha = -1/2$)					
655.6	2528.0	$23/2^-$	$19/2^-$	30(4)	1.2(4)
679.4	3207.4	$27/2^-$	$23/2^-$	90(10)	
702.4	3909.8	$31/2^-$	$27/2^-$	60(6)	0.8(1)
740.8	4650	$35/2^-$	$31/2^-$	50(5)	1.2(4)
778.0	5428	$39/2^-$	$35/2^-$	30(5)	1.0(3)
830.3	6258		$39/2^-$	15(10)	
$\alpha = +1/2$					
137.0	523.9	$5/2^-$	$(1/2^-)$	15(5)	
235.0	758.9	$9/2^-$	$5/2^-$	80(10)	1.1(1)
358.1	1117.0	$13/2^-$	$9/2^-$	120(10)	0.99(6)
482.3	1599.3	$17/2^-$	$13/2^-$	150(8)	1.01(2)
587.2	2186.5	$21/2^-$	$17/2^-$	155(8)	0.98(9)
663.1	2849.6	$25/2^-$	$21/2^-$	145(8)	1.1(2)
702.3	3551.9	$29/2^-$	$25/2^-$	90(5)	1.0(1)
730.2	4282.1	$33/2^-$	$29/2^-$	55(3)	0.9(2)
775.3	5057.4	$37/2^-$	$33/2^-$	25(3)	
841.8	5898	$41/2^-$	$37/2^-$	20(3)	
920.3	6818	$45/2^-$	$41/2^-$	15(3)	
1006.2	7824	$49/2^-$	$45/2^-$	8(2)	
1087.8	8912	$53/2^-$	$49/2^-$	6(2)	
1181.7	10094	$57/2^+$	$53/2^-$	4(2)	
Other transitions related to band 4 ($\alpha = +1/2$)					
719.2	2905.2	$29/2^-$	$25/2^-$	30(3)	1.1(2)
740.4	3645.6	$33/2^-$	$29/2^-$	20(3)	1.0(2)
795.4	4441.0	$37/2^-$	$33/2^-$	15(5)	0.9(3)
$\Delta I = 1$ *transitions*					
170.3	523.9	$5/2^-$	$3/2^-$	55(5)	1.21(7)
266.3	758.9	$9/2^-$	$7/2^-$	35(10)	1.0(15)
308.5	1117.0	$13/2^-$	$11/2^-$	25(10)	0.85(2)
Band 5: Highly deformed band					
345.3	2372.4	$21/2^+$	$17/2^+$	70(8)	1.0(2)
440.9	2813.3	$25/2^+$	$21/2^+$	120(10)	0.9(2)
514.1	3327.4	$29/2^+$	$25/2^+$	130(10)	1.0(2)
604.3	3931.7	$33/2^+$	$29/2^+$	190(15)	1.0(2)
683.5	4615.2	$37/2^+$	$33/2^+$	180(15)	1.2(3)
761.8	5377.0	$41/2^+$	$37/2^+$	160(15)	0.9(2)
835.6	6212.6	$45/2^+$	$41/2^+$	145(10)	1.0(2)
903.6	7116.2	$49/2^+$	$45/2^+$	125(10)	1.1(2)
967.0	8083.2	$53/2^+$	$49/2^+$	105(10)	1.2(4)
1029.2	9112.4	$57/2^+$	$53/2^+$	80(10)	0.9(2)
1092.4	10204.8	$61/2^+$	$57/2^+$	60(7)	0.9(2)
1158.7	11363.5	$65/2^+$	$61/2^+$	37(5)	1.2(3)

TABLE I. (*Continued*).

E_γ (keV)	E_i (keV)	I_i	I_f	Intensity	R_{DCO}
1228.0	12591.5	$69/2^+$	$65/2^+$	33(5)	0.9(2)
1300.9	13892.4	$73/2^+$	$69/2^+$	15(5)	1.0(2)
1378.0	15270.4	$77/2^+$	$73/2^+$	17(5)	
1458.0	16728.4	$81/2^+$	$77/2^+$	9(5)	
1545.2	18273.6	$85/2^+$	$81/2^+$	5(3)	
1632.1	19905.7	$89/2^+$	$85/2^+$	5(3)	
Band 6					
$\alpha = +1/2$					
270.0	398.0	$5/2^+$	$1/2^+$	50(10)	1.1(1)
427.6	825.6	$9/2^+$	$5/2^+$	75(15)	1.0(2)
534.3	1359.9	$13/2^+$	$9/2^+$	85(5)	1.1(1)
603.2	1963.1	$17/2^+$	$13/2^+$	50(5)	
590.9	2554.0	$21/2^+$	$17/2^+$	15(3)	
575.1	3129.1	$25/2^+$	$21/2^+$	10(3)	
635.7	3764.8	$29/2^+$	$25/2^+$	10(3)	
704.2	4469.0	$33/2^+$	$29/2^+$	10(3)	
742.0	5211.0	$37/2^+$	$33/2^+$	5(3)	
758.0	5969.0	$41/2^+$	$37/2^+$	5(3)	
$\alpha = -1/2$					
318.9	492.2	$7/2^+$	$3/2^+$	160(20)	0.94(4)
471.0	963.2	$11/2^+$	$7/2^+$	150(15)	0.94(7)
577.8	1541.0	$15/2^+$	$11/2^+$	140(8)	1.02(3)
619.5	2160.5	$19/2^+$	$15/2^+$	130(7)	1.0(1)
605.2	2765.7	$23/2^+$	$19/2^+$	70(7)	0.89(9)
654.2	3419.9	$27/2^+$	$23/2^+$	20(3)	1.2(2)
705.1	4125.0	$31/2^+$	$27/2^+$	20(3)	1.0(2)
753.5	4878.5	$35/2^+$	$31/2^+$	20(5)	
790.3	5668.8	$39/2^+$	$35/2^+$	10(3)	
$\Delta I = 1$ *transitions*					
225.0	398.0	$5/2^+$	$3/2^+$	55(5)	1.12(5)
333.6	825.6	$9/2^+$	$7/2^+$	10(3)[a]	1.09(12)
396.9	1359.9	$13/2^+$	$11/2^+$	10(3)	1.01(3)
422.3	1963.1	$17/2^+$	$15/2^+$	5(3)	1.05(7)
Band 7					
$\alpha = +1/2$					
495.4	3271.4	$(27/2^+)$	$23/2^+$	25(5)	
670.2	3941.9	$(31/2^+)$	$(27/2^+)$	30(5)	1.1(2)
785.3	4726	$(35/2^+)$	$(31/2^+)$	20(5)	1.6(4)
834.0	5560	$(39/2^+)$	$(35/2^+)$	10(3)	
$\alpha = -1/2$					
750.6	4347	$(33/2^+)$	$(29/2^+)$	10(3)	
810	5157	$(37/2^+)$	$(33/2^+)$	10(3)	0.7(3)
$\Delta I = 1$ *transitions*					
216.6	2992.5	$25/2^+$	$23/2^+$	30(5)	0.27(6)
278.9	3271.4	$(27/2^+)$	$25/2^+$	25(5)	0.53(4)
325.5	3396.9	$(29/2^+)$	$(27/2^+)$	30(5)	0.52(7)
345.0	3941.9	$(31/2^+)$	$(27/2^+)$	30(5)	0.49(8)
405.0	4346.9	$(33/2^+)$	$(31/2^+)$	10(3)	
379.1	4726.0	$(35/2^+)$	$(33/2^+)$	10(3)	
431	5157	$(37/2^+)$	$(35/2^+)$	5(3)	
(403)	5560	$(39/2^+)$	$(37/2^+)$	5(3)	
Other transitions related to band 7					
643.8	3419.8	$27/2^+$	$23/2^+$	15(5)	1.1(2)
730.2	4150.0		$27/2^+$	5(3)	

TABLE I. (*Continued*).

E_γ (keV)	E_i (keV)	I_i	I_f	Intensity	R_{DCO}
Band 8					
$\alpha = +1/2$					
396.4	687.9	$9/2^+$	$5/2^+$	40(10)	1.10(13)
443.0	1130.9	$13/2^+$	$9/2^+$	65(10)	1.7(2)[b]
493.0	1623.9	$17/2^+$	$13/2^+$	70(10)	
688.8	2312.7	$21/2^+$	$17/2^+$	50(10)	
777.8	3090.5	$25/2^+$	$21/2^+$	10(5)	
$\alpha = -1/2$					
429.8	913.6	$11/2^+$	$7/2^+$	50(10)	1.8(2)[b]
452.5	1366.1	$15/2^+$	$11/2^+$	50(10)	0.94(10)
570.8	1936.9	$19/2^+$	$15/2^+$	50(10)	
740.9	2677.8	$23/2^+$	$19/2^+$	50(10)	
$\Delta I = 1$ transitions					
192.3	483.8	$7/2^+$	$5/2^+$	45(10)	0.60(3)
204.3	687.9	$9/2^+$	$7/2^+$	30(10)	0.39(7)
225.6	913.6	$11/2^+$	$9/2^+$	50(10)	1.2(2)[b]
217.5	1130.9	$13/2^+$	$11/2^+$	45(10)	1.0(2)[b]
235.1	1366.1	$15/2^+$	$13/2^+$	35(10)	0.9(2)[b]
258.0	1623.9	$17/2^+$	$15/2^+$	30(10)	1.1(2)[b]
313	1936.9	$19/2^+$	$17/2^+$	10(5)	
(377)	2312.7	$21/2^+$	$19/2^+$		
Band 9					
$\alpha = +1/2$					
581.4	827.0	$13/2^+$	$9/2^+$	500(25)	1.11(9)
665.0	1492.0	$17/2^+$	$13/2^+$	490(25)	0.91(6)
597.5	2089.5	$21/2^+$	$17/2^+$	445(20)	0.94(15)
604.7	2694.2	$25/2^+$	$21/2^+$	420(40)	0.99(15)
672.0	3366.2	$29/2^+$	$25/2^+$	240(15)	1.0(1)
712.2	4078.4	$33/2^+$	$29/2^+$	130(7)	0.8(2)
782.8	4861.2	$37/2^+$	$33/2^+$	65(5)	
851.9	5713.1	$41/2^+$	$37/2^+$	55(10)	
906.6	6619.7	$45/2^+$	$41/2^+$	45(10)	
967.5	7587.2	$49/2^+$	$45/2^+$	15(5)	
1035.6	8622.8	$53/2^+$	$49/2^+$	15(5)	
1106.9	9729.7	$57/2^+$	$53/2^+$	15(5)	
1183.5	10913.2	$61/2^+$	$57/2^+$	10(5)	
1266	12179	$65/2^+$	$61/2^+$		
$\alpha = -1/2$					
519.5	519.5	$11/2^+$	$7/2^+$	380(25)	0.95(6)
631.0	1150.5	$15/2^+$	$11/2^+$	480(25)	0.92(6)
648.6	1799.1	$19/2^+$	$15/2^+$	440(23)	0.91(6)
585.5	2384.6	$23/2^+$	$19/2^+$	400(23)	0.96(6)
636.1	3020.7	$27/2^+$	$23/2^+$	375(20)	0.90(6)
694.7	3715.4	$31/2^+$	$27/2^+$	270(15)	1.1(1)
743.4	4458.8	$35/2^+$	$31/2^+$	165(10)	0.9(3)
821.0	5279.8	$39/2^+$	$35/2^+$	50(3)	0.9(3)
879.1	6158.9	$43/2^+$	$39/2^+$	(70)[a]	
937.1	7096.0	$47/2^+$	$43/2^+$	(70)[a]	
1001.7	8097.7	$51/2^+$	$47/2^+$	33(5)	
1072.0	9169.7	$55/2^+$	$51/2^+$	20(5)	
1146.6	10316.3	$59/2^+$	$55/2^+$	20(5)	
1224.5	11540.8	$63/2^+$	$59/2^+$	10(5)	
1300	12841	$67/2^+$	$63/2^+$	5(3)	
$\Delta I = 1$ transitions					
245.6	245.6	$9/2^+$	$7/2^+$	575(35)	0.41(3)

TABLE I. (*Continued*).

E_γ (keV)	E_i (keV)	I_i	I_f	Intensity	R_{DCO}
274.0	519.5	$11/2^+$	$9/2^+$	125(10)	0.51(6)
307.4	827.0	$13/2^+$	$11/2^+$	50(3)	
323.6	1150.5	$15/2^+$	$13/2^+$	40(3)	0.2(1)
341.5	1492.0	$17/2^+$	$15/2^+$	40(3)	0.46(6)
307.0	1799.1	$19/2^+$	$17/2^+$	105(7)	
290.5	2089.5	$21/2^+$	$19/2^+$	125(7)	0.56(6)
295.3	2384.6	$23/2^+$	$21/2^+$	140(8)	0.56(6)
309.6	2694.2	$25/2^+$	$23/2^+$	140(8)	
326.6	3020.7	$27/2^+$	$25/2^+$	80(5)	0.65(6)
345.5	3366.2	$29/2^+$	$27/2^+$	80(5)	0.3(1)
349.3	3715.4	$31/2^+$	$29/2^+$	75(5)	
363.0	4078.4	$33/2^+$	$31/2^+$	40(3)	
380.5	4458.8	$35/2^+$	$33/2^+$	35(3)	
402.6	4861.2	$37/2^+$	$35/2^+$	20(3)	
418.5	5279.8	$39/2^+$	$37/2^+$		
Other transitions related to band 9					
269.2	2946.9				
741.0	2677.7		$19/2^+$		
755.6	4121.8		$29/2^+$	90(5)	
786.2	1936.7		$15/2^+$		
796.2	4511.6		$31/2^+$	45(3)	
820.8	2312.8		$17/2^+$	110 (20)	
806	4927			40(5)	
856.7	5368.3			25(3)	
878.4	2677.7		$19/2^+$	20(3)	
914	5841				
Interband transitions					
Band 1 → Band 2					
141.3	3168.9	$27/2^-$	$27/2^-$	20(3)	1.5(2)
149.2	3168.9	$27/2^-$	$(23/2^-)$	15(5)	0.7(1)
374.2	3401.9	$29/2^-$	$27/2^-$	120(5)	0.3(2)
631.2	3659.3	$31/2^-$	$27/2^-$	45(3)	0.8(1)
969.0	3168.9	$27/2^-$	$23/2^-$	280(10)	1.06(6)
1009.0	3019.9	$(23/2^-)$	$21/2^-$	15(5)	
1020.3	3031.0	$25/2^-$	$21/2^-$	65(5)	1.1(7)
Band 2 → Band 9					
176.3	176.3	$9/2^-$	$7/2^+$		
Band 4 → Band 2					
316.1	492.6	$7/2^-$	$9/2^-$		
Band 4 → Band 6					
180.8	353.6	$3/2^-$	$3/2^+$	15(5)	0.75(6)
258.5	386.9	$(1/2^-)$	$1/2^+$		
HD band → other bands					
306.6	3327.4	$29/2^+$	$27/2^+_{\text{band 9}}$	10(3)	
409.1	2372.4	$21/2^+$	$17/2^+_{\text{band 6}}$	50(6)	1.03(9)
486.2	2027.1	$17/2^+$	$15/2^+_{\text{band 6}}$	5(3)	0.8(1)
500.1	2372.4	$21/2^+$	$19/2^-_{\text{band 4}}$	10(3)	0.71(5)
565.6	3931.7	$33/2^+$	$29/2^+_{\text{band 9}}$	14(4)	
633.2	3327.4	$29/2^+$	$25/2^+_{\text{band 9}}$	50(6)	1.06(9)
667.1	2027.1	$17/2^+$	$13/2^+_{\text{band 6}}$	40(6)	0.9(1)
723.7	2813.3	$25/2^+$	$21/2^+_{\text{band 9}}$	5(2)	
746.3	2027.1	$17/2^+$	$15/2^-_{\text{band 4}}$	10(3)	0.75(11)
1189.7	2027.1	$17/2^+$	$15/2^-_{\text{band 2}}$	10(3)	
Band 6 → HD band					
527.0	2554.0	$21/2^+$	$17/2^+$	5(3)	

TABLE I. (*Continued*).

E_γ (keV)	E_i (keV)	I_i	I_f	Intensity	R_{DCO}
Band 6 → Band 8					
200.7	492.2	$7/2^+$	$5/2^+$	20(3)	0.42(6)
342.0	825.6	$9/2^+$	$7/2^+$	25(5)	0.60(6)
479.5	963.2	$11/2^+$	$7/2^+$	15(3)	1.0(2)
(534)	825.6	$9/2^+$	$5/2^+$		
(672)	1359.9	$13/2^+$	$9/2^+$		
Band 7 → Band 6					
226.7	2992.5	$25/2^+$	$23/2^+$	40(5)	0.50(25)
615.5	2776.0	$23/2^+$	$19/2^+$	60(20)	1.0(1)
Band 8 → Band 6					
118.5	291.5	$5/2^+$	$3/2^+$		2.5(4)[b]
196.1	687.9	$9/2^+$	$7/2^+$	30(5)	0.56(9)
310.2	483.8	$7/2^+$	$3/2^+$	30(5)	
Band 8 → Band 9					
291.5	291.5	$5/2^+$	$7/2^+$	125(15)	0.8(8)
442.5	687.9	$9/2^+$	$9/2^+$		
483.8	483.8	$7/2^+$	$7/2^+$	45(5)	
Band 9 → HD band					
553.1	3366.2	$29/2^+$	$25/2^+$	5(3)	1.0(1)
Band 9 → Band 8					
433.3	1799.1	$19/2^+$	$15/2^+$	55(3)	
465.5	2089.5	$21/2^+$	$17/2^+$	50(3)	

[a]Doublet.

[b]DCO ratio obtained by gating on a dipole transition.

In its IBFM-1 version, this model does not distinguish between the neutron and proton degrees of freedom. The ^{132}Nd nucleus was chosen as core of ^{133}Nd, and described by an IBM-1 parametrization very close to that used for ^{128}Ba and ^{130}Ce in Refs. [23,24]. The odd fermion was allowed to occupy the four positive parity valence orbitals specified above. The IBFM-1 Hamiltonian [21] consists of the IBM-1 Hamiltonian of the even-even core, a single-nucleon energy term, and a boson-fermion interaction term (V_{BF}). The latter contains a monopole-monopole, a quadrupole-quadrupole, and an exchange interaction, respectively:

$$V_{BF} = V_0 + V_{qq} + V_{exch}, \qquad (1)$$

where

$$V_0 = \sum_j A_j [(d^\dagger \tilde{d})^{(0)} (a_j^\dagger \tilde{a}_j)^{(0)}]_0^{(0)},$$

$$V_{qq} = \sum_{jj'} \Gamma_{jj'} [Q_B^{(2)} (a_j^\dagger \tilde{a}_{j'})^{(2)}]_0^{(0)},$$

$$V_{exch} = \sum_{jj'} \sum_{j''} \Lambda_{jj'}^{j''} : [(d^\dagger \tilde{a}_j)^{j''} (\tilde{d} a_{j'}^\dagger)^{j''}]_0^{(0)} :.$$

$d^\dagger$ and $a_j^\dagger$ are the usual d-boson and fermion creation operators, respectively, $Q_B^{(2)}$ is the IBM quadrupole operator, and the sums run over the valence orbitals j considered. By using a simplified form based on microscopic arguments [31], the boson-fermion interaction is fully determined by three parameters A_0, Γ_0, and Λ_0, which specify the strengths of the monopole, quadrupole, and exchange terms, respectively. Both the IBFM Hamiltonian and the electromagnetic transition operators have been chosen as in the previous calculations for ^{129}Ba [23] and ^{131}Ce [24]. Thus, the boson-fermion interaction strengths were $A_0 = -0.15$ MeV, $\Gamma_0 = 0.49$ MeV, and $\Lambda_0 = 0.5$ MeV. In this way, no parameters were adjusted and this calculation had a predictive character. The results are shown in Fig. 5. The calculations provide the three low-lying positive parity band structures (below the backbend) which have been observed experimentally [bands 6, 8, and 9 in Fig. 3(b)]. Their relative positions are not perfectly reproduced but the calculations can be easily improved from this point of view by slightly readjusting the single particle energies of the considered spherical shell model orbitals. On the other hand, the decay modes (branching ratios) of these bands are reasonably well reproduced.

The structure of the calculated states is as follows. Band 9 [see Fig. 3(b)] is dominated by the spherical $g_{7/2}$ orbital coupled to the states of the core ground-state band, whereas band 8 is dominated by the spherical $d_{5/2}$ orbital (which gives a 80% contribution) with a smaller component (20%) from the $g_{7/2}$ orbital. Finally, band 6 is a mixture between the $s_{1/2}$ and $d_{3/2}$ orbitals, with the two signature partners being dominated one by the $s_{1/2}$ orbital (the $\alpha = 1/2$ one), and the other by the $d_{3/2}$ orbital. The calculations predict some connections between the ''$d_{5/2}$'' and ''$g_{7/2}$'' bands. Experimentally these linking transitions were not observed due, most likely, to the fact that the ''$d_{5/2}$'' band is very weakly populated. These wave function compositions correspond indeed, qualitatively, to the Nilsson assignments shown in Fig. 3(b).
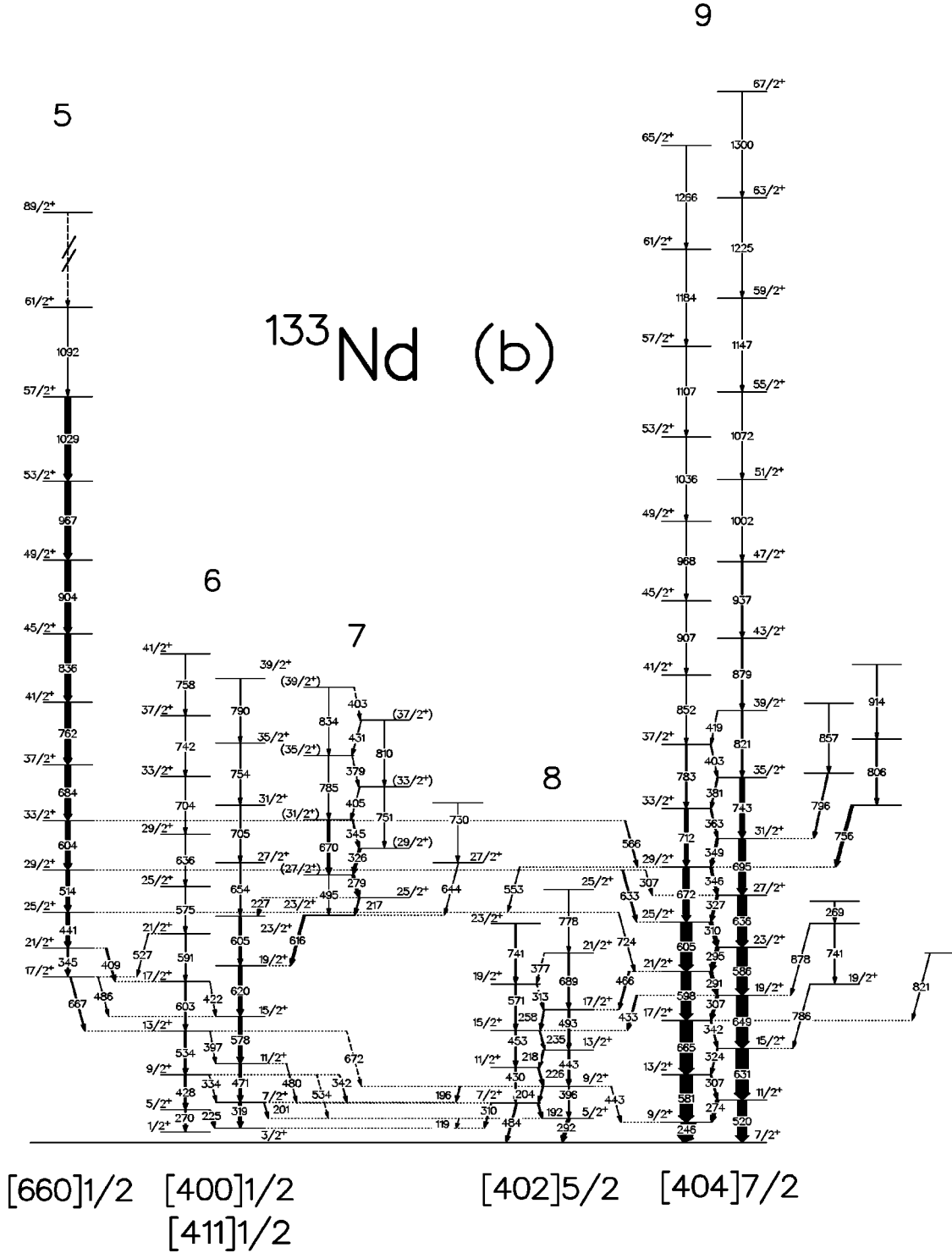
FIG. 3. (a) Negative parity band structures in ^{133}Nd observed in the present experiments: the positive parity HD (band 5) is also shown partially (only its lowest portion) to illustrate its decay to the positive parity levels. The dominant Nilsson configuration assigned to each band is indicated. (b) Positive parity band structures in ^{133}Nd observed in the present experiments. The dominant Nilsson configuration assigned to each band is indicated.

One may conclude at this point that the lowest part of the positive-parity band structures observed in ^{133}Nd is reasonably well understood on the basis of a multishell IBFM-1 calculation with the same parameters that were previously used to describe its isotones ^{129}Ba and ^{131}Ce. One should add that we have also verified that the calculation of Ref. [23] describes well the more recent, richer experimental data obtained in the meantime for ^{129}Ba [25].

A similar approach to the negative-parity states is only partly successful. Both in Ba and Ce isotopes the bands based on the unique parity orbital $h_{11/2}$ can be easily de-

scribed by IBFM calculations with appropriate parameters [23,24], and a similar approach for ^{133}Nd provides a good description for band 2. In the isotonic Ba and Ce nuclei, however, the other, low-K band, originating from the intruder $h_{9/2}$ orbital has not been observed. Such a band cannot be predicted at low excitation energy on the basis of an IBFM calculation performed, as usually, using a realistic set of spherical single-particle levels. The reproduction of the low-lying part of band 4 in such a calculation would require at least a large *ad hoc* lowering of the $h_{9/2}$ single-particle energy, which is difficult to justify.

FIG. 3. (*Continued.*)

B. Particle-plus-triaxial-rotor model and cranked shell-model interpretation

1. Model description and calculation procedures

In order to describe the low-lying structures in ^{133}Nd PTRM calculations have been performed applying the formalism of [20]. The rotor-plus-particle Hamiltonian has the form

$$H = \sum_{k=1}^{3} (I_k^2 - 2I_k j_k + j_k^2)/2\Theta_k + H_{\text{part}}(\varepsilon_2, \gamma). \quad (2)$$

I_k and j_k are the projections of the total angular momentum and of the particle angular momentum, respectively, on the intrinsic axes. In this Hamiltonian the particle-rotation interaction emerges in the form of a Coriolis term $-\Sigma I_k j_k / \Theta_k$ and a recoil term $\Sigma j_k^2 / 2\Theta_x$.

The moments of inertia of the rigid core Θ_k are given by the hydrodynamical formula

$$\Theta_k = \frac{4}{3} \Theta_0 \sin^2\left(\gamma + \frac{2}{3}\pi k \right). \quad (3)$$
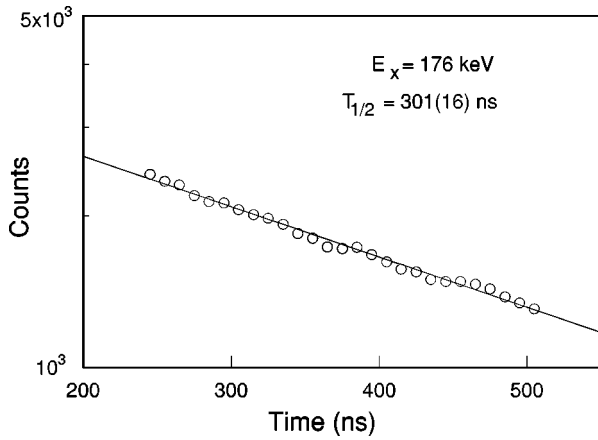
FIG. 4. Decay curve of the $E_x = 176$ keV isomer obtained in the thick target experiment. The experimental error bars are within the drawn symbols. The error given for the half-life is larger than the statistical one, and corresponds mainly to the uncertainty in the background of the time spectrum.

The particle Hamiltonian $H_{part}(\varepsilon_2, \gamma)$ describes the particle motion in a Nilsson potential with deformation parameters ε_2 and γ. For the oscillator potential parameters κ and μ the standard values given in [32] have been used. Pairing was treated in the usual way within the BCS approximation with standard value for the pairing strength [33].

In the negative-parity state calculations, the $1h_{11/2}$, $2f_{7/2}$, and $1h_{9/2}$ single-particle orbitals have been considered, while in the positive-parity state calculations all the $N=4$ single-

particle orbitals were included. Calculations were performed using either a constant or a variable moment of inertia for the core. In the first case the parameter Θ_0 was calculated for a core excitation energy $E(2^+) = 200$ keV close to the experimental energy of 213 keV of the first 2^+ state in the neighboring even-even ^{132}Nd nucleus. Another model parameter, the coefficient ξ representing the attenuation of the Coriolis matrix elements, has been varied between 1 (no attenuation) and 0.6. In evaluation of the electromagnetic moments, an effective g_s factor of $0.6g_s^{free}$ has been used and g_R has been taken as Z/A. Quadrupole moments of the core were calculated macroscopically. For the quadrupole deformation parameter of the harmonic oscillator potential a value of $\varepsilon_2 = 0.23$ has been used, which corresponds, according to [33], to the deformation $\beta_2 = 0.26$ derived from recently reported lifetime measurements in the low-lying bands of ^{133}Nd [34]. The calculations have been done for a wide range of γ values. Optimum values of this parameter have been determined from the comparison of the experimental and calculated level energies. We have to point out that in the PTRM the triaxial deformation parameter characterizing the rigid core has positive values ranging from $\gamma = 0°$ (prolate shape) to $\gamma = 60°$ (oblate shape). They correspond to the interval of negative γ values $0°--60°$ in the Lund convention, which we will follow in the paper.

In the CSM analysis the cranking formalism outlined in Ref. [35] has been applied to transform the experimental excitation energies and spins of the bands into Routhians and alignments as a function of rotational frequency ω. The ref-
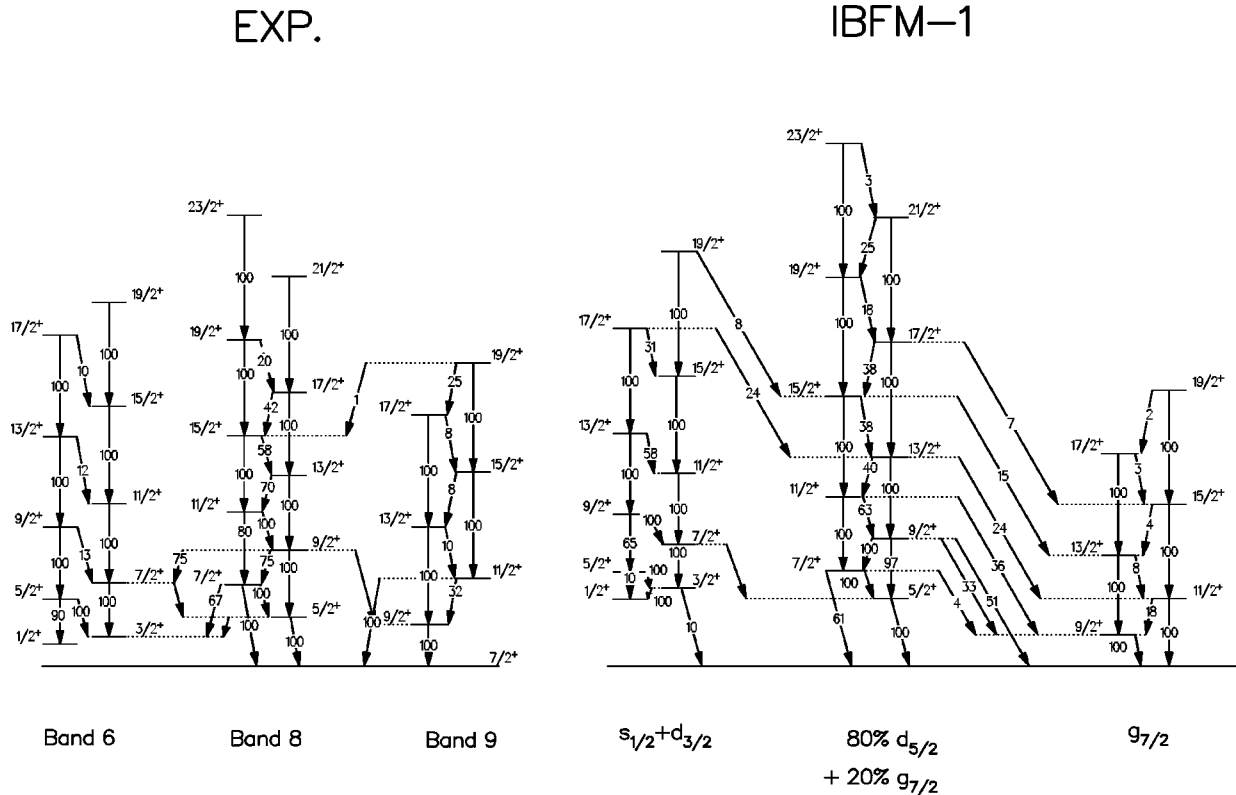
FIG. 5. Comparison between the lowest part of the positive parity band structures with IBFM-1 calculations. The arrows show the most important γ-ray decays, with the branching ratios indicated (for each level the strongest branch is taken 100). The experimental bands are marked with their numbering of Fig. 3, whereas for the calculated ones the dominant spherical shell-model configuration is indicated (see text for details).
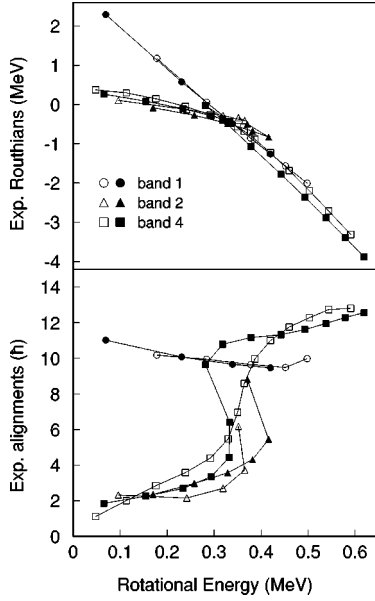
FIG. 6. Experimental Routhians and alignments of the negative parity band structures of ^{133}Nd. A reference with the Harris parameters $J_0 = 17.0 \ \hbar^2 \mathrm{MeV}^{-1}$ and $J_1 = 25.8 \ \hbar^4 \mathrm{MeV}^{-3}$ has been subtracted. The K values assumed correspond to the Nilsson assignments shown in Fig. 3(a). Open symbols correspond to signature $\alpha = +1/2$, filled ones to $\alpha = -1/2$.

erence Harris parameters $J_0 = 17.0 \ \hbar^2 \mathrm{MeV}^{-1}$ and $J_1 = 25.8$ $\hbar^4 \mathrm{MeV}^{-3}$, obtained from fitting the levels of the ^{130}Ce S band [36], have been used for all the bands. The ^{130}Ce S band reference has been preferred to the ^{132}Nd ground-state band reference because we aim to apply the CSM to states at frequencies higher than the first band crossing, where a reference obtained from the fit of the three lowest states in ^{132}Nd would be less suitable [37]. The same Harris parameters have been used to describe a large number of S bands in the Xe-Ba-Ce isotopes [38] and in Nd isotopes [39]. The discussion below will be of course only qualitative, due to the fact that in a γ-soft region the deformation can change slightly from a band to another. The experimental Routhians and alignments are shown in Fig. 6 for the negative-parity bands and in Fig. 7 for the positive-parity bands.

CSM and total Routhian surface (TRS) calculations have been performed using a Woods-Saxon potential with monopole pairing interaction described in [4]. Figure 8 shows calculated Routhians for both proton and neutron quasiparticles in ^{133}Nd, at deformations $\beta_2 = 0.25$ and $\beta_4 = 0.01$, for $\gamma = 0°$ and $\gamma = -20°$. In the notation adopted the lowest energy neutron (proton) orbitals of positive parity are labeled a, b, c, ... $(A, B, C, \ldots)$, while the corresponding negative-parity orbitals are labeled e, f, g, ... $(E, F, G, \ldots)$.

Valuable information about the structure and the deformation of the bands was provided by the analysis of the reduced transition probabilities ratios, $B(M1)/B(E2)$. The experimental ratios $B(M1)/B(E2)$ have been derived from the γ-ray branching ratios using the relation

$$\frac{B(M1)}{B(E2)} = 0.6967 \frac{E_\gamma^5(I \rightarrow I-2)}{E_\gamma^3(I \rightarrow I-1)} \frac{1}{\lambda(1+\delta^2)}, \quad (4)$$
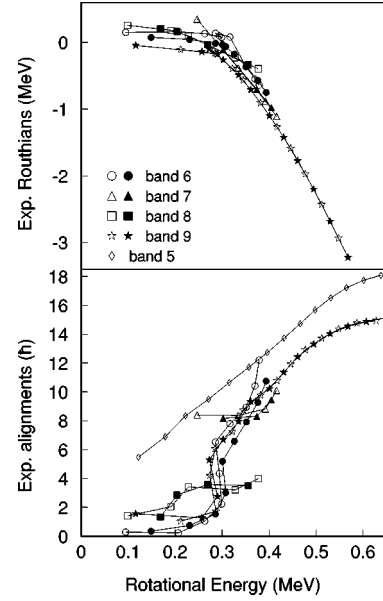
FIG. 7. Same as in Fig. 6, but for the positive parity band structures of ^{133}Nd. The alignment determined for the HD band 5 is also given for comparison, in the region of frequencies of the other bands.

where the γ-ray energies E_γ are given in MeV, $\lambda = I_\gamma(I \rightarrow I-2)/I_\gamma(I \rightarrow I-1)$ is the branching ratio, and δ is the $E2/M1$ mixing ratio. The correction for the mixing ratios could be important for low-lying transitions, especially in strongly coupled bands. In the present case however mixing ratios were determined experimentally only for few transitions. We have therefore evaluated them from the measured branching ratios using the rotational model relation [40], assuming pure K:
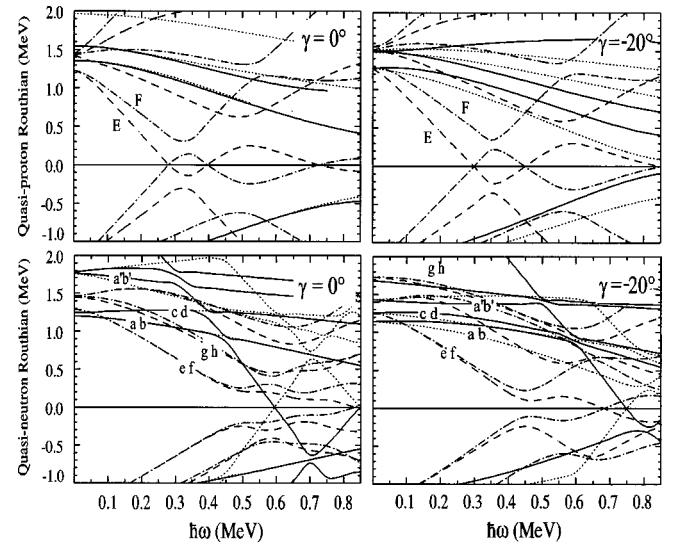
FIG. 8. Single quasiparticle Routhians for protons (top) and neutrons (bottom) in ^{133}Nd, calculated at $\beta_2 = 0.25$, $\beta_4 = 0.01$ and for γ values of 0° (left) and $-20°$ (right). The following line convention has been used in the Routhian diagram: π:$+$, $\alpha = +1/2$ solid, π:$+$, $\alpha = -1/2$ dotted, π:$-$, $\alpha = +1/2$ dashed-dotted, and π:$-$, $\alpha = -1/2$ dashed line.
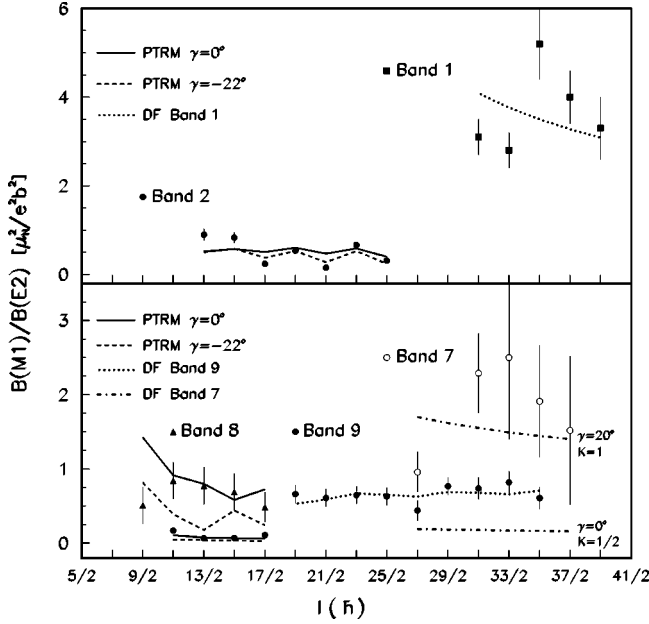
FIG. 9. Experimental $B(M1)/B(E2)$ values (filled and open symbols) for several bands in ^{133}Nd compared to the calculated values (lines) using the PTRM and the DF formula. Empirical g factors were used for the single-particle configurations as follows: $g(\nu h_{11/2})=-0.2$, $g(\nu g_{7/2})=+0.27$, $g(\nu s_{1/2})=-1.3$, $g(\nu d_{3/2})=+0.6$, $g(\pi h_{11/2})=+1.25$.

$$\frac{1}{\delta^2} = \frac{1}{\lambda} \frac{E_\gamma^5(I\to I-2)}{E_\gamma^5(I\to I-1)} \frac{\langle IK20|I-2K\rangle^2}{\langle IK20|I-1K\rangle^2} - 1, \quad (5)$$

and from PTRM calculations using the theoretical reduced transition probabilities and the experimental energies for the $I\to I-1$ transitions. The δ values derived by the two procedures were quite similar.

The $B(M1)/B(E2)$ values determined for the high-spin structures above particle alignment were interpreted under the assumption af axial symmetry by means of the semiclassical Dönau-Frauendorf (DF) formula [41,42]:

$$\frac{B(M1)}{B(E2)} = \frac{16}{5Q_0^2} \frac{K^2}{I^2} (1-K^2/I^2)^{-2} \{(g_n-g_R)$$
$$\times [(I^2-K^2)^{1/2}-i_n]-(g_{\text{align}}-g_R)i_{\text{align}}\}^2, \quad (6)$$

where g_n and i_n are the g factor and the alignment of the valence neutron, while g_{align} and i_{align} are the same quantities for the aligned particles. The quadrupole moment $Q_0=4.8$ eb, derived from lifetime measurements [34], was used in all calculations. The experimental ratios $B(M1)/B(E2)$ are shown in Fig. 9 together with the theoretical estimates obtained within the PTRM for the lower part of the bands below the particle alignment and with the DF formula for the bands above it. The g factors for quasiparticle excitations were taken from the compilation of Ref. [43]. In the following we shall analyze the observed bands using both the PTRM and CSM predictions.
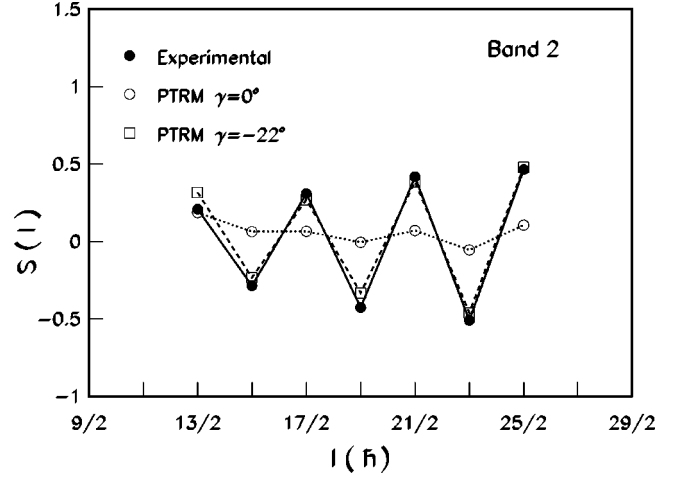
FIG. 10. Experimental signature splitting for band 2 in ^{133}Nd compared with PTRM calculations using two different values for the triaxiality parameter γ.

2. Negative-parity bands

We will first discuss the negative-parity bands of ^{133}Nd displayed in Fig. 3(a). One has to point out that collective structures rather similar to bands 1, 2, and 3 in ^{133}Nd have been also observed in both ^{129}Ba [25] and ^{131}Ce isotones [27].

a. Band 2. Band 2 is the yrast one and the most strongly populated at low spin. Few transitions belonging to it were first reported in Ref. [9] where an interpretation was given within the model of Meyer-ter-Vehn [12] by assuming a large triaxiality. This band, showing strong signature splitting, is built on the $9/2^-$ $T_{1/2}=301$ ns isomer, described by a configuration involving the mixing of intrinsic orbitals from the $h_{11/2}$ neutron j shell, with a dominant [514]9/2 component. Our present PTRM calculations have confirmed the extreme sensitivity of the signature splitting of the yrast negative-parity levels on the γ deformation. The signature splitting function $S(I)$ defined as [44]

$$S(I) = \frac{E(I)-E(I-1)}{E(I)-E(I-2)} \frac{I(I+1)-(I-2)(I-1)}{I(I+1)-I(I-1)} - 1, \quad (7)$$

is illustrated in Fig. 10 for the experimental and PTRM calculated levels of band 2. The observed splitting cannot be explained assuming axial symmetry, but it is very well reproduced with a value of $\gamma=-22°$. The optimum γ value was found to be slightly dependent on the values used for the moment of inertia and the attenuation of the Coriolis interaction, a variation by no more than $\pm2°$ being obtained at reasonable changes of these PTRM parameters. Similar to the ^{129}Ba [18] and ^{131}Ce [19] isotones, the description of the level energies has been considerably improved when an attenuation of the Coriolis matrix elements was included, the optimum value being found for $\xi=0.8$. The experimental staggering in this band is decreasing slightly along the isotonic chain, corresponding to a decrease of about 15% in the γ value from ^{129}Ba to ^{133}Nd. We note that the experimental $B(M1)/B(E2)$ ratios in the band are also better reproduced by PTRM calculations with triaxiality (see Fig. 9).

TRS calculations predict, as lowest in energy, a configuration with $\beta_2 = 0.256$ and $\beta_4 = 0.01$ characterized by γ softness at low rotational frequency (i.e., below the alignment), which corresponds to the e, f trajectories in Fig. 8. Both signatures of this band show the beginning of a large alignment at $\hbar\omega \approx 0.4$ MeV, apparently keeping the large signature splitting (see Fig. 6). The experimental alignment is well described by assuming the configuration $\nu [514]9/2$ for the band. A similar jump in alignment at $\hbar\omega \approx 0.4$ MeV has been observed also in the isotones ^{131}Ce [27] and ^{129}Ba [25], and is interpreted as the alignment of a pair of $h_{11/2}$ neutrons, which polarizes the core even more towards an oblate shape. Only a few other candidates for the crossing between the one-quasiparticle $\nu h_{11/2}$ band and the three-quasiparticle $\nu (h_{11/2})^3$ band have been found in the Xe, Ba, and Ce isotopes [45], where a TRS analysis has also shown that the crossing frequency of these configurations depends very sensitively on the γ parameter.

b. Band 1. Band 1 has a large initial alignment gain (Fig. 6) and no signature splitting. These facts strongly suggest the alignment of a pair of $h_{11/2}$ protons, which should take place at a frequency of about 0.3 MeV (E, F trajectories in Fig. 8) to the $\nu h_{11/2}$ configuration. The protons and neutrons in the $h_{11/2}$ orbital are polarizing the nucleus towards positive and negative γ-deformations, respectively [46] and therefore the three-quasiparticle $\nu h_{11/2} \otimes \pi (h_{11/2})^2$ configuration is expected to have a prolate shape with no signature splitting. TRS calculations predict indeed the same β_2 and β_4 values and $\gamma = 0°$ above this alignment. The band 1 behaves very similarly to the band V in ^{131}Ce [27] and band 1 in ^{129}Ba [25] which are also interpreted as having a three-quasiparticle configuration $\nu h_{11/2} \otimes \pi (h_{11/2})^2$. In ^{129}Ba the band shows a small signature splitting [25], interpreted as evidence of triaxiality with positive γ deformation. This feature points to an increased γ softness for the ^{129}Ba isotone. On the other side, the quadrupole moment $Q_0 = 3.4$ eb deduced on the basis of static quadrupole moment [43] and lifetime measurements [47] indicates a lower quadrupole deformation for ^{129}Ba when compared with ^{133}Nd. The larger deformation in ^{133}Nd seems to stabilize the shape against γ softness. The assigned configuration is supported by the $B(M1)/B(E2)$ ratios. As seen in Fig. 9, the large experimental $B(M1)/B(E2)$ values are rather well described by the estimates obtained with the Dönau-Frauendorf formula for $K = 9/2$ and $i_{\text{align}} = 10\hbar$.

c. Band 3. There is a short $\Delta I = 2$ cascade, band 3, also assigned as a negative-parity structure, namely a sequence of states with spins 15/2, 19/2, 23/2, feeding the $13/2^-$ state of the $[514]9/2$ band, by a 539 keV transition. Our PTRM calculations performed with $\gamma = -22°$ have reproduced very well these yrare states of the $\nu h_{11/2}$ configuration, the calculated energy being 493 keV for the $15/2_2 \rightarrow 13/2_1$ transition. The band is predicted much higher in energy by the calculations with $\gamma = 0°$, the energy for the $15/2_2 \rightarrow 13/2_1$ transition being 1294 keV in this case. The occurrence of this band gives therefore further support to the triaxial shape associated to the $\nu h_{11/2}$ configuration. Similar results were found in recent PTRM calculations with large γ for ^{129}Ba [18] and ^{131}Ce [19]. In both ^{129}Ba and ^{131}Ce this structure is fed by the $\nu h_{11/2} \otimes \pi (h_{11/2})^2$ one and has more than one link with

the $\nu h_{11/2}$ structure. In ^{133}Nd we have found only the lowest transition which connects it to the $\nu h_{11/2}$ band. In addition, in our case this structure feeds, and is fed by, the $[541]1/2$ band [Fig. 3(a)].

d. Band 4. Several low-lying members of band 4 have been observed in the β decay of ^{133}Pm and have been interpreted within the PTRM as part of the intruder $[541]1/2$ band [28]. We note that the new $(1/2^-)$ state placed at $E_x = 387$ keV in the present work fits nicely with the predictions of the PTRM calculations which indicate that the $1/2^-$ state should lie very close to the $3/2^-$ level (see Fig. 9 of Ref. [28]). Our PTRM calculations performed at $\gamma = 0°$ are very similar to those reported in [28]. A mixed single-particle wave function, with almost equal amplitudes for the $\Omega = 1/2$ states ($[541]1/2$ and $[530]1/2$) from the $h_{9/2}$ and $f_{7/2}$ orbitals, has been obtained for this band and the observed level sequence has been well described by the PTRM calculations.

Up to now ^{133}Nd is the only odd-mass, odd-N nucleus in the region where this intruder band has been identified. On the other hand, such a structure has been recently studied in the $Z = 73$ ^{171,173}Ta isotopes [29,30]. In these latter cases, the band exhibits a decoupled feature, with the unfavored partner pushed at higher energy. It was interesting to see if this different behavior compared to ^{133}Nd could be described by particle-rotor calculations. For this purpose a PTRM calculation for ^{173}Ta has been performed, using $\epsilon_2 = 0.26$ and $\gamma = 0°$. A much purer single-particle wave-function, dominated by the $h_{9/2}$ orbital, has been calculated for the intruder band, and the decoupled character observed experimentally has been nicely reproduced.

Band 4 is predicted to be axially symmetric by TRS calculations with a small shape coexistence at $\beta_2 = 0.29$. The somewhat larger deformation compared to the other low-lying bands was confirmed by recent lifetime measurements [34,48]. The CSM diagrams of Fig. 8 describe reasonably the experimental situation. We assign this band to the g, h trajectories in Fig. 8, which come very close to the $h_{11/2}$ band (e, f) for β_2 deformations larger than 0.24. The single-particle alignment of about $2.0\hbar$ at $\hbar\omega \approx 0.2$ MeV is comparable with the value observed experimentally. Below the backbending this band has a rather large signature splitting. Slightly above $\hbar\omega = 0.30$ MeV, it experiences the alignment of a $\pi h_{11/2}$ proton pair, and above the alignment it still preserves a sizeable signature splitting. No $\Delta I = 1$ transitions have been observed experimentally above the alignment, indicating $M1$ branching lower than 5%. This feature is in accordance with the DF formula, which predict extremely small $B(M1)/B(E2)$ values for this $K = 1/2$ band in spite of the large g factor of the aligned protons.

3. Positive-parity bands

a. The highly-deformed band. The properties of the HD band and of its decay out have been discussed in detail in Refs. [10,11]. The quadrupole deformation of the band is calculated to be $\beta_2 \approx 0.35$ [4,10], a value which has been confirmed experimentally [5,34,48]. On the other side, the quadrupole deformation of the normal deformed rotational bands has been measured to be $\beta_2 \approx 0.25$ [34]. A peculiar aspect of the HD band of ^{133}Nd, as well as of some other nuclei in the region, is the rather smooth alignment process,
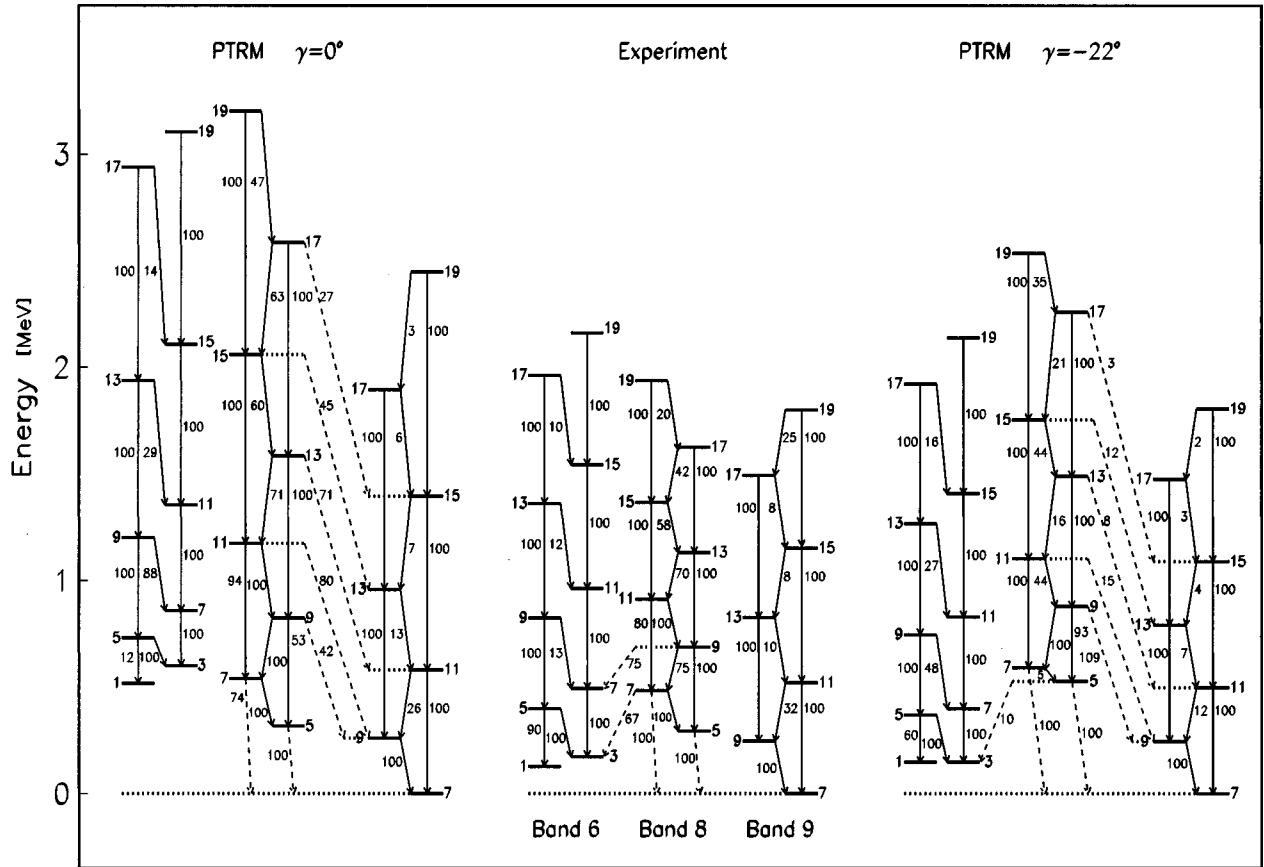
FIG. 11. Comparison between the experimental and the calculated positive-parity low-lying bands. The core energy $E(2^+) = 200$ keV has been used for moment of inertia calculations. No attenuation of the Coriolis interaction has been applied ($\xi = 1$). The theoretical branchings were obtained using the reduced $B(M1)$ and $B(E2)$ transition probabilities derived by PTRM and the experimental transition energies. The levels are labeled with twice the value of their spin.

visible by the hump in the dynamical moment of inertia $J^{(2)}$ at $\hbar\omega = 0.5$ MeV, which has been associated with the $h_{11/2}$ proton crossing. Self-consistent cranked Strutinski calculations, based on a Woods-Saxon potential and including monopole pairing correlations, were performed in the attempt to reproduce the experimentally determined $J^{(1)}$ and $J^{(2)}$ moments of inertia [10]. Those calculations were not able to reproduce the data, encountering serious problems with the $\pi h_{11/2}$ alignment, predicted to occur at a frequency 0.1 MeV lower. Recently, more realistic, self-consistent TRS calculations, including a separable pairing force of the monopole plus quadrupole type [49], have been performed for the HD band in ^{133}Nd, which reproduce quite well the $\pi h_{11/2}$ alignment within this band (see Fig. 3 in Ref. [49]).

b. The normally-deformed bands. The experimental excitation energies and branching of the low-lying positive-parity bands are compared in Fig. 11 with the results of our PTRM calculations performed at $\gamma = 0°$ and $\gamma = -22°$. The value $\gamma = -22°$ gives the best description of band 2 (as shown above) and also of band 6 (see below).

Band 6. A good description of band 6 is provided by the PTRM assuming triaxiality (see Fig. 11). In particular, the bandhead excitation energy is very well reproduced by calculations at $\gamma = -22°$, while for $\gamma = 0°$ it is predicted too high. The structure of this $K = 1/2$ band involves a mixing of components coming from the $s_{1/2}$ and $d_{3/2}$ neutron orbitals. Similar conclusions concerning triaxiality have been ob-

tained from the analyses of the corresponding $K = 1/2$ band in ^{129}Ba [50] and ^{131}Ce [19]. In ^{129}Ba the $1/2^+$ state becomes the ground state, which indicates a somewhat larger γ value, similarly to the [514]9/2 band. In the case of ^{133}Nd the band has been followed at much higher spins. The band can be assigned as the a', b' positive-parity Routhians in Fig. 8 which reproduce the signature splitting of about 100 keV around the 0.2 MeV frequency and have the $\alpha = -1/2$ signature as favored in energy. Above $\hbar\omega \simeq 0.3$ MeV, band 6 shows a peculiar alignment increase (see Fig. 7) which could be attributed to the $\nu h_{11/2}$ alignment, since no blocking is expected for this configuration.

Band 7. Band 7, characterized by a large alignment (see Fig. 7), feeds band 6 in a similar way as band 1 feeds band 2. It is therefore natural to suggest a similar mechanism of proton alignment as in the case of band 2 where the γ-soft nucleus is driven to a prolate shape. The band starts as a regular band, in spite of the fact that for a $K = 1/2$ band one usually expects signature splitting at $\gamma = 0°$. The absence of a relevant signature splitting could be due to a compensation of the decoupling effects of the $s_{1/2}$ and $d_{3/2}$ components. Rather large $B(M1)/B(E2)$ ratios (although with big errors) have been experimentally found as shown in Fig. 9, giving support to the proton alignment picture. The DF formula (3) predicts however $B(M1)/B(E2)$ values which are much lower than the measured ones (see Fig. 9). In order to explain the large experimental $B(M1)/B(E2)$ values, one could as-

sume that the band has a larger effective K value due to Coriolis mixing and/or that some triaxiality is present at high spins due to the driving force of $h_{11/2}$ protons towards positive γ. We applied the DF formula (3) in which the Q_0^2 was replaced by $Q_0^2 \cos^2(\gamma+30°)/\cos^2(30°)$ and, as seen in Fig. 9, a satisfactory agreement with the experimental data was reached for $K=1$ and $\gamma=20°$. We mention however that the proposed interpretation is only qualitative, as the application of the DF formula for mixed bands or in the case of triaxial shapes is only a rough approximation. In this band there is an indication of a crossing with a 5-qp band, at a frequency of about 0.4 MeV, which is likely due to the alignment of two $\nu h_{11/2}$ neutrons.

Band 8. The structure of band 8 is dominated by the [402]5/2 neutron orbital with small mixing (less than 10%) of the [404]7/2 neutron orbital. PTRM calculations indicate an overall agreement assuming axial symmetry. Both the bandhead excitation energy and the $B(M1)/B(E2)$ ratios are better reproduced at $\gamma=0°$ (see Figs. 9 and 11). Moreover one can see that the triaxiality would induce signature splitting, in disagreement with the observed regularity of the band. The somewhat smaller energies of the transitions in the experimental band compared to the PTRM predictions at $\gamma=0°$ indicate a larger moment of inertia compared to that of the neighboring even-even nucleus. Such effects were observed also in the ground-state bands of Ce isotopes [19]. Similar to the IBFM calculations, the PTRM calculations predict $\Delta I=1$ transitions from this band to the ground-state band levels. As already mentioned, such links were not observed experimentally as the band 8 is very weakly populated.

TRS calculations predict for this band an axially symmetric shape. The Routhian of band 8 can be identified with trajectories *c, d* in Fig. 8, corresponding to the [402]5/2 orbital. The band could not be observed up to very high spins. No structure similar to this band has been identified in the ^{129}Ba and ^{131}Ce isotones.

Band 9. As seen in Fig. 11, band 9 (the ground-state band) is rather well described by PTRM with both $\gamma=0°$ and $\gamma=-22°$. The experimental branching are in agreement with those calculated at $\gamma=0°$. Similar to band 8, a better description of the level energies could be obtained at $\gamma=0°$ with a higher moment of inertia or with VMI.

The band is predicted to be axially symmetric by TRS calculations. This band, having the lowest energy Routhian, an initial alignment of about $1\hbar$ and no signature splitting, can be readily identified with the *a, b* orbitals (see Fig. 8) which correspond to the [404]7/2 Nilsson configuration. The alignment plot shows a peculiar behavior which is quite different from that displayed in the ^{129}Ba and ^{131}Ce isotones [25,27]. In both these nuclei only the crossing at $\simeq 0.3$ MeV with the $\nu g_{7/2} \otimes \pi(h_{11/2})^2$ 3-qp band is observed, perhaps followed by the beginning of the $\nu(h_{11/2})^2$ alignment at $\simeq 0.55$ MeV in ^{129}Ba [25]. In the present case, as shown in the alignment plot of Fig. 7, shortly after the $\pi h_{11/2}$ pair alignment (at about 0.35 MeV) a smooth alignment gain starts. The behavior of the $B(M1)/B(E2)$ ratios for this band is also quite different from that observed in ^{129}Ba. In ^{129}Ba this ratio has very small values below the backbend and it jumps at values of 3–4 $\mu_N^2/e^2 b^2$ above the backbend;

this effect was shown to be consistent only with the $\pi(h_{11/2})^2$ alignment assuming also a positive triaxiality $\gamma = 20°$ [25]. In our case (Fig. 9), small $B(M1)/B(E2)$ values were also found before the backbend whereas for the region of frequencies from about 0.3 to 0.4 MeV values of 0.5–0.7 $\mu_N^2/e^2 b^2$ have been determined. We have applied the Dönau-Frauendorf formula (3) assuming the $\nu[404]7/2 \otimes \pi(h_{11/2})^2$ configuration and taking the experimental alignments (gradually increasing from a value of $i_{align} \approx 4\hbar$ at $I=19/2$ to a value of $i_{align} \approx 10\hbar$ at $I=35/2$, see Fig. 7). The calculated $B(M1)/B(E2)$ ratios reproduce well the experimental behavior, as seen in Fig. 9. The alignment plot suggests a strong interaction of the ground-state band with the $h_{11/2}$ proton pair band, which can be considered as an indication for an axial symmetric shape, while the γ-soft bands 2 and 6 present a weak interaction. The smooth alignment gain observed after the $\pi h_{11/2}^2$ alignment may indicate some overlapping with a second alignment, probably due to neutrons.

Such smooth alignment behavior of band 9 has been discussed in some detail in Ref. [10] and alternatively attributed to a change from the configuration with $\beta_2=0.25$ encountered at the lowest frequencies, to a more deformed one ($\beta_2=0.30$) in which two nonaligned neutrons were promoted from the Nilsson orbital [402]5/2 (immediately below the Fermi surface) into the $h_{9/2}$ orbital which becomes yrast in the region of frequencies of the proton alignment. This assignment is also supported by the observed interaction between the levels of band 9 in this region ($I \approx 25/2\hbar$) and the highly deformed intruder band (band 5) which involves also two $h_{9/2}$ neutrons in a nonaligned configuration [10]. This description should be tested experimentally through DSAM lifetime measurements at high spin.

It is worthwhile to mention that a shape-change mechanism similar to that presented above has been recently discussed in the $Z=73$ ^{173}Ta nucleus, in order to explain the gradual upbend observed experimentally in the alignment of the [404]7/2 band [30]. Like in ^{133}Nd, the shape change has been attributed to the crossing with a more-deformed band containing a pair of spin-zero coupled particles (protons in the ^{173}Ta case) in the $h_{9/2}$ orbital.

V. CONCLUSIONS

In this paper we have presented and discussed the level scheme of ^{133}Nd obtained in a series of experiments performed with the GASP spectrometer. The well known HD rotational band has been firmly linked to the other excited states at normal deformation. The rich variety of band structures observed has been interpreted according to various theoretical models, which had demonstrated their validity in the $A=130$ mass region. In particular, a good description of the low-lying states of the positive-parity bands has been given by the IBFM. More extensive PTRM calculations reproduce quite nicely many properties of both positive- and negative-parity low lying states, giving evidence of the coexistence, at low spin, of bands (built on intrinsic states) with different triaxial and/or axially symmetric shapes. The high spin part of the level scheme, including the HD rotational band, is interpreted in the framework of the CSM and TRS calculations.

The data obtained in the present Au-backed target mea-

surement as well as those of Gd-backed target experiment [8] have been analyzed by using the Doppler-shift attenuation method, for lifetime determination in the rotational bands. The results of this analysis will be presented in a forthcoming paper.

[1] P.J. Nolan, D.J.G. Love, A.H. Nelson, D.J. Unwin, and P.J. Twin, J. Phys. G **11**, L17 (1985).

[2] R. Wadsworth, A. Kirwan, D.J.G. Love, Y-X Luo, J-Q Zhong, P.J. Nolan, P.J. Bishop, M.J. Godfrey, R. Hughes, A.N. James, I. Jenkins, S.M. Mullins, J. Simpson, D.J. Thornley, and K.L. Ying, J. Phys. G **13**, L207 (1987).

[3] E.M. Beck, R.J. McDonald, A.O. Macchiavelli, J.L. Bacelar, M.A. Deleplanque, R.M. Diamond, J.E. Draper, and F.S. Stephens, Phys. Lett. B **195**, 531 (1987).

[4] R. Wyss, J. Nyberg, A. Johnson, R. Bengtsson, and W. Nazarewicz, Phys. Lett. B **215**, 211 (1988).

[5] S.M. Mullins, I. Jenkins, Y-J. He, A.J. Kirwan, P.J. Nolan, J.R. Hughes, R. Wadsworth, and R.A. Wyss, Phys. Rev. C **45**, 2683 (1992).

[6] G. Viesti, T. Negro, D. Bazzacco, R. Burch, G. de Angelis, M. De Poli, D. Fabris, E. Fioretto, S. Lunardi, G. Nebbia, G. Prete, J. Rico, and C. Rossi Alvarez, Nucl. Phys. **A579**, 225 (1994).

[7] S.A. Forbes, G. Böhm, R.M. Clark, A. Dewald, R. Krücken, S.M. Mullins, P.J. Nolan, P.H. Regan, and R. Wadsworth, Z. Phys. A **352**, 15 (1995).

[8] N.H. Medina, F. Brandolini, D. Bazzacco, P. Pavan, C. Rossi Alvarez, R. Burch, S. Lunardi, R. Menegazzo, M. De Poli, G. Maron, R.V. Ribas, and M. Ionescu-Bujor, Nucl. Phys. **A589**, 106 (1995).

[9] Y. Choquer, A. Gizon, and J. Gizon, J. Phys. (Paris) **38**, L157 (1977).

[10] D. Bazzacco, F. Brandolini, R. Burch, A. Buscemi, C. Cavedon, G. De Acuna, S. Lunardi, R. Menegazzo, P. Pavan, C. Rossi Alvarez, M. Sferrazza, R. Zanon, G. de Angelis, P. Bezzon, M.A. Cardona, M. De Poli, G. Maron, M.L. Mazza, D. Napoli, J. Rico, P. Spolaore, X.N. Tang, G. Vedovato, N. Blasi, I. Castiglioni, G. Falconi, G. LoBianco, P.G. Bizzeti, and R. Wyss, Phys. Lett. B **309**, 235 (1993).

[11] D. Bazzacco, F. Brandolini, S. Lunardi, E. Maglione, N.H. Medina, P. Pavan, C. Rossi Alvarez, G. De Acuna, M. De Poli, J. Rico, D. Bucurescu, and C.A. Ur, Phys. Rev. C **49**, R2281 (1994).

[12] J. Meyer-ter-Vehn, Nucl. Phys. **A249**, 111 (1975).

[13] J. Gizon, A. Gizon, and J. Meyer-ter-Vehn, Nucl. Phys. **A277**, 464 (1977).

[14] J. Gizon and A. Gizon, Z. Phys. A **285**, 259 (1978).

[15] J. Gizon, A. Gizon, R.M. Diamond, and F.S. Stephens, Nucl. Phys. **A290**, 272 (1977).

[16] J. Yan, O. Vogel, P. von Brentano, and A. Gelberg, Phys. Rev. C **48**, 1046 (1993).

[17] D. Lieberz, A. Gelberg, P. von Brentano, I. Ragnarsson, and P.B. Semmes, Phys. Lett. B **282**, 7 (1992).

[18] A. Gelberg, D. Lieberz, P. von Brentano, I. Ragnarsson, P.B. Semmes, and I. Wiedenhöver, Nucl. Phys. **A557**, 439c (1993).

[19] M. Ionescu-Bujor, A. Iordachescu, F. Brandolini, M. De Poli, N.H. Medina, P. Pavan, M.N. Rao, and C. Rossi Alvarez, Nucl. Phys. **A633**, 459 (1998).

[20] S.E. Larsson, G. Leander, and I. Ragnarsson, Nucl. Phys. **A307**, 189 (1978).

[21] F. Iachello and P. Van Isacker, in *The Interacting Boson-Fermion Model* (Cambridge University Press, Cambridge, 1991).

[22] G. Căta-Danil, D. Bucurescu, A. Gizon, and J. Gizon, J. Phys. G **20**, 1051 (1994).

[23] D. Bucurescu, G. Căta-Danil, N.V. Zamfir, A. Gizon, and J. Gizon, Phys. Rev. C **43**, 2610 (1991).

[24] A. Gizon, J. Genevey, D. Bucurescu, G. Căta-Danil, J. Gizon, J. Gizon, J. Inchaouh, D. Barneoud, T. von Egidy, C.F. Liang, B.M. Nyako, P. Paris, I. Penev, A. Plochocki, E. Rokowska, C.A. Ur, B. Weiss, and L. Zolnai, Nucl. Phys. **A605**, 301 (1996).

[25] A.P. Byrne, K. Schiffer, G.D. Dracoulis, B. Fabricius, T. Kibédi, A.E. Stuchbery, and K.P. Lieb, Nucl. Phys. **A548**, 131 (1992).

[26] K.S. Krane, R.M. Steffen, and R.M. Wheeler, Nucl. Data Tables **111**, 351 (1973).

[27] M. Palacz, Z. Sujkowski, J. Nyberg, J. Bacelar, J. Jongman, W. Urban, W. Hesselink, J. Nasser, A. Plompen, and R. Wyss, Z. Phys. A **338**, 467 (1991).

[28] J.B. Breitenbach, J.L. Wood, M. Jarrio, R.A. Braga, K. Kormicki, and P.B. Semmes, Nucl. Phys. **A592**, 194 (1995).

[29] J.C. Bacelar, R. Chapman, J.R. Leslie, J.C. Lisle, J.N. Mo, E. Paul, A. Simcock, J.C. Willmott, J.D. Garrett, G.B. Hagemann, B. Herskind, A. Holm, and P.M. Walker, Nucl. Phys. **A442**, 547 (1985).

[30] H. Carlsson, R.A. Bark, L.P. Ekström, A. Nordlund, H. Ryde, G.B. Hagemann, S.J. Freeman, H.J. Jensen, T. Lönnroth, M.J. Piiparinen, H. Schnack-Petersen, F. Ingebretsen, and P.O. Tjøm, Nucl. Phys. **A592**, 89 (1995).

[31] O. Scholten, Ph.D. thesis, University of Groningen, 1980.

[32] T. Bengtsson and I. Ragnarsson, Nucl. Phys. **A436**, 14 (1985).

[33] S.G. Nilsson, C.F. Tsang, A. Sobiczewski, Z. Szymański, S. Wycech, C. Gustafsson, I.-L. Lamm, P. Möller, and B. Nilsson, Nucl. Phys. **A131**, 1 (1969).

[34] R. Peusquens, A. Dewald, S. Kasemann, R. Krücken, H. Tiesler, K.O Zell, P. von Brentano, P. Petkov, S. Lunardi, D. Bazzacco, F. Brandolini, N.H. Medina, P. Pavan, C.M. Petrache, C. Rossi Alvarez, G. de Angelis, G. Maron, and D.R. Napoli,

LNL-INFN Annual Report 1996, p. 31.

[35] R. Bengtsson and S. Frauendorf, Nucl. Phys. **A327**, 139 (1979).

[36] D.M. Todd, R. Aryaeinejad, D.J.G. Love, A.H. Nelson, P.J. Nolan, P.J. Smith, and P.J. Twin, J. Phys. G **10**, 1407 (1984).

[37] R. Bengtsson, S. Frauendorf, and F.-R. May, At. Data Nucl. Data Tables **35**, 15 (1986).

[38] R. Wyss, A. Granderath, R. Bengtsson, P. von Brentano, A. Dewald, A. Gelberg, A. Gizon, J. Gizon, S. Harissopulos, A. Johnson, W. Lieberz, W. Nazarewicz, J. Nyberg, and K. Schiffer, Nucl. Phys. **A505**, 337 (1989).

[39] R. Wyss, Ph.D. thesis, Stockholm University, 1990.

[40] G.B. Hagemann, J.D. Garrett, B. Herskind, G. Sletten, P.O. Tjøm, A. Henriquez, F. Ingebretsen, J. Rekstad, G. Løvhøiden, and T.F. Thorsteinsen, Phys. Rev. C **25**, 3224 (1982).

[41] F. Dönau and S. Frauendorf, *High Angular Momentum Properties of Nuclei*, edited by N.R. Johnson (Harwood, New York, 1983), p. 143.

[42] F. Dönau, Nucl. Phys. **A471**, 469 (1987).

[43] P. Raghavan, At. Data Nucl. Data Tables **42**, 189 (1989).

[44] N.V. Zamfir and R. Casten, Phys. Lett. B **200**, 265 (1991).

[45] A. Granderath, P. F. Mantica, R. Bengtsson, R. Wyss, P. von Brentano, A. Gelberg, and F. Seiffert, Nucl. Phys. **A597**, 427 (1996).

[46] Y.S. Chen, S. Frauendorf, and G.A. Leander, Phys. Rev. C **28**, 2437 (1983).

[47] A. Dewald (private communication).

[48] N. H. Medina, F. Brandolini, D. Bazzacco, D. Bucurescu, G. de Angelis, M. De Poli, A Dewald, G. Falconi, M. Ionescu-Bujor, S. Lunardi, D. Napoli, R. Menegazzo, G. Pascovici, P. Pavan, R. V. Ribas, C. Rossi Alvarez, C. A. Ur, and W. Wilhelm, *Proceedings of the 2nd Latin American Workshop on Nuclear and Heavy Ion Physics*, Caracas (Venezuela), 1997, Acta Physica Ungarica, New Series, Heavy Ion Physics **7** (1998).

[49] W. Satula and R. Wyss, Acta Phys. Pol. B **27**, 121 (1996).

[50] A.C. Müller, F. Buchinger, W. Klempt, E.W. Otten, R. Neugart, C. Ekström, J. Heinemeier, and the ISOLDE Collaboration, Nucl. Phys. **A403**, 234 (1983).